

Static and dynamical quantum correlations in phases of an alternating-field XY model

Titas Chanda, Tamoghna Das, Debasis Sadhukhan, Amit Kumar Pal, Aditi Sen(De), and Ujjwal Sen
Harish-Chandra Research Institute, Chhatnag Road, Jhansi, Allahabad 211019, India
and Homi Bhabha National Institute, Training School Complex, Anushaktinagar, Mumbai-400094, India
 (Received 11 July 2016; published 7 October 2016)

We investigate the static and dynamical patterns of entanglement in an anisotropic XY model with an alternating transverse magnetic field, which is equivalent to a two-component one-dimensional Fermi gas on a lattice, a system realizable with current technology. Apart from the antiferromagnetic and paramagnetic phases, the model possesses a dimer phase which is not present in the transverse XY model. At zero temperature, we find that the first derivative of bipartite entanglement can detect all the three phases. We analytically show that the model has a “factorization line” on the plane of system parameters, in which the zero-temperature state is separable. Along with investigating the effect of temperature on entanglement in a phase plane, we also report a nonmonotonic behavior of entanglement with respect to temperature in the antiferromagnetic and paramagnetic phases, which is surprisingly absent in the dimer phase. Since the time dynamics of entanglement in a realizable physical system plays an important role in quantum information processing tasks, the evolutions of entanglement at small as well as large time are examined. Consideration of large-time behavior of entanglement helps us to prove that in this model, entanglement is always ergodic. We observe that other quantum correlation measures can qualitatively show similar features in zero and finite temperatures. However, unlike nearest-neighbor entanglement, the nearest-neighbor information-theoretic measures can be both ergodic as well as nonergodic, depending on the system parameters.

DOI: [10.1103/PhysRevA.94.042310](https://doi.org/10.1103/PhysRevA.94.042310)

I. INTRODUCTION

Quantum many-body systems have been established to be a possible candidate for the implementation of quantum information protocols [1,2] such as one-way quantum computation [3] and network quantum communication [4]. Also, laboratory realization of model Hamiltonians in various substrates, including optical lattice [5–7], ion traps [2,8], solid-state systems [9], and nuclear magnetic resonance (NMR) [10], have made possible the testing of properties of several information theoretic measures of quantum correlations, belonging to both of the entanglement-separability [11] and information-theoretic [12] domains. On the other hand, tools developed in, and with the help of, quantum information theory have been found to be useful in the analysis of the ground and excited states of such many-body systems [13–15]. Moreover, development of topological quantum computation and especially topological quantum memories indicate the importance of quantum many-body systems in the goal of practical realization of a quantum computer [16]. Consequently, in recent years, characterization of quantum many-body systems from quantum information-theoretic perspectives has become a vibrant field of research.

Although most of such studies are restricted to the “static” properties of quantum correlations in the zero-temperature and thermal states, the time evolution of the system is also extremely important in quantum information processing tasks like in one-way quantum computation [3]. In the static case, the traditional approach to study a quantum many-body system is to recognize appropriate order parameters defining the phases occurring in the system, and to investigate the response of these order parameters to external perturbations. The ground state of such a system is usually represented by a complex multipartite quantum state, characterized by the classical as well as the quantum correlations present between its constituting parts. A quantum phase transition (QPT) [17,18], which occurs at zero temperature and solely due to quantum fluctuations, brings about a qualitative change

in the ground state of a quantum many-body system, when a system parameter is varied. Quantum correlations having quantum information-theoretic origins are shown to be useful in characterizing various phases and corresponding QPTs in a large spectrum of quantum many-body systems [19–28] (see also [1,12], and the references therein). Among all these models, a prominent one is the one-dimensional (1D) Fermi gas of spinless fermions in an optical lattice, a system realizable in ultracold atom substrate, by using a Fermi-Bose mixture in the strong-coupling limit [29]. In the spin language, the model can be described by an anisotropic XY model in a transverse magnetic field [17,18,30,31].

Manipulation of cold atoms in the laboratory has allowed the realization of physical systems such as dilute atomic Fermi and Bose gases, in different spatial dimensions, thereby providing excellent opportunities to apply quantum information-theoretic concepts in these systems [32,33]. Recent experimental evidences of superfluid, metallic, and Mott-insulating phases [34,35] motivate one to investigate a Fermi gas of spinless fermions in a 1D optical lattice, where the fermions are of two types, distinguished by different chemical potentials. Considering the two types of fermions to be located on two different sublattices, one of which contains all the “even” sites and the other one holds all the “odd” ones, the fermionic model, via a Jordan-Wigner transformation, can be shown to be equivalent to a 1D anisotropic XY model in the presence of a uniform, and an alternating transverse magnetic field that alternates its direction from $+z$ to $-z$ depending on whether the lattice site is even or odd [18,36–39]. The model offers a rich phase diagram. While only two phases, viz., a “paramagnetic” (PM) phase and an “antiferromagnetic” (AFM) phase, occur in the ground state of the XY model in a uniform transverse field [17,30,31], an additional “dimer” (DM) phase emerges due to the introduction of the local site-dependent alternating field in the present model [18,36–39]. Although the properties of several quantum information-theoretic measures of quantum correlations have

been extensively studied and reported for different phases and corresponding QPTs in the former case [21–23] (see also Refs. [1,12]), it is interesting to see how this phase structure, formed due to the introduction of the alternating field, can be characterized using quantum correlations. In this paper, we characterize the static as well as dynamic properties of quantum correlations in the 1D anisotropic XY model in a uniform and an alternating field. As the measures of quantum correlations, we focus on bipartite measures, and use logarithmic negativity (LN) [40] from the entanglement-separability genre and quantum discord (QD) [42,43] from the information-theoretic domain. We show that irrespective of the values of the anisotropy parameter, the first derivative of bipartite entanglement can detect all the three phases in this model. Moreover, the finite-size scaling analysis of the system near the QPTs is performed to distinguish phase boundaries between the AFM and the PM, and between the AFM and the DM. Similar investigations are also carried out for quantum discord, which also faithfully indicate the quantum critical points. Like the factorization point in the XY model [44,45], we here prove the existence of a line in the space of the system parameters, which we call as the “factorization line” (FL), on which the ground state of the system is separable, having a Néel-type order.

The change of phase diagram with finite temperature has both fundamental and experimental importance due to the technological limitations of reaching absolute zero temperature. In this scenario, we discuss the weathering of the landscapes of quantum correlations over the phase plane of the system parameters, chosen to be the strengths of the uniform and the alternating transverse field, with increasing temperature. We point out that bipartite entanglement is the most fragile in the AFM phase, while it is robust in the DM phase against increasing temperature. We identify the phases in which nonmonotonicity of entanglement with the increase of temperature is observed. Specifically, we perform a nonmonotonicity cartography, and map, on the plane of the chosen system parameters, the regions in which the thermal quantum correlations exhibit nonmonotonic variation with temperature. We show that for LN and for high values of anisotropy parameter, most of the nonmonotonicity occurs in the AFM region, while QD is found to be nonmonotonic in the PM phase for low anisotropy. Interestingly, we discover that the temperature variation of LN is found to be monotonic in the entire DM phase, while for QD, nonmonotonicity occurs at a very small region of the DM phase.

As already stated, the time dynamics of quantum correlations in any physical system is extremely relevant for implementation of quantum information processing tasks. In this paper, we find both the small- and large-time quantum correlation patterns of the evolved state. We observe that although entanglement dies quickly compared to QD, it possesses larger value than QD, which ensures the possibility of implementing several information tasks requiring high values of entanglement. The study of large-time behavior of quantum correlations also helps us to settle issues like the ergodicity [46–54] of LN and QD, quantified by the ergodicity scores. We find that, up to our numerical accuracy, entanglement always remains ergodic, while QD shows nonergodicity in different phases of the model. We point out that the region of nonergodicity of QD increases with an increase in the anisotropy in the system.

Therefore, with respect to transverse field parameter, we show that QD undergoes a nonergodic to ergodic transition which is absent for entanglement up to our numerical accuracy, irrespective of the anisotropy parameter and initial temperature.

The paper is organized as follows. In Sec. II, the Hamiltonian describing the anisotropic XY model in the presence of a uniform and an alternating transverse field and its relation to a two-component 1D Fermi gas are discussed. Brief descriptions on the diagonalization of the model Hamiltonian and the different phases occurring in the ground state of the model are provided in the same section. Section III contains the definitions of the canonical equilibrium state and the time-evolved state of the system. The determination of the single-site and two-site reduced density matrices from the canonical equilibrium state and the time-evolved state of the model is also presented in this section. The static properties of the quantum correlations, including the different types of QPTs, finite-size scaling analysis, determination of the factorization line, and thermal quantum correlations are discussed in Sec. IV. Section V reports the ergodicity of quantum correlations and short-time dynamics of entanglement as well as QD. Section VI contains the concluding remarks.

II. MODEL

Let us consider a family of models describing a system of spins of magnitude $\frac{1}{2}$ on a 1D lattice consisting of N sites. We assume that an external transverse magnetic field of site-dependent strength $h_i(t) = h_1(t) + (-1)^i h_2(t)$, i being the site index, acts on the spins at time t . The magnetic field can be interpreted as the resultant of a uniform transverse field $h_1(t)$ and a transverse field $h_2(t)$, which reverses its direction from $+z$ to $-z$, depending on whether the lattice site is even or odd. The Hamiltonian describing the system is given by

$$\hat{H} = \frac{1}{2} \sum_{i=1}^N \left\{ J \left(\frac{1+\gamma}{2} \hat{\sigma}_i^x \hat{\sigma}_{i+1}^x + \frac{1-\gamma}{2} \hat{\sigma}_i^y \hat{\sigma}_{i+1}^y \right) + [h_1(t) + (-1)^i h_2(t)] \hat{\sigma}_i^z \right\}. \quad (1)$$

Here, the system parameter J represents the strength of the exchange interaction, while $\gamma (\neq 0)$ is the $x - y$ anisotropy present in the system. We assume periodic boundary condition (PBC), and an even number of lattice sites, such that $\hat{\sigma}_{N+1}^\alpha \equiv \hat{\sigma}_1^\alpha$, where $\alpha = x, y, z$.

A. Relation to one-dimensional Fermi gas

The Hamiltonian in Eq. (1), via a Jordan-Wigner transformation, given by [38]

$$\begin{aligned} \hat{\sigma}_{2j}^+ &= \hat{b}_{2j}^\dagger \exp \left(i\pi \sum_{l=1}^{j-1} \hat{b}_{2l}^\dagger \hat{b}_{2l} + i\pi \sum_{l=1}^j \hat{a}_{2l-1}^\dagger \hat{a}_{2l-1} \right), \\ \hat{\sigma}_{2j+1}^+ &= \hat{a}_{2j+1}^\dagger \exp \left(i\pi \sum_{l=1}^j \hat{b}_{2l}^\dagger \hat{b}_{2l} + i\pi \sum_{l=0}^{j-1} \hat{a}_{2l+1}^\dagger \hat{a}_{2l+1} \right), \end{aligned} \quad (2)$$

can be mapped onto a two-component Fermi gas of spinless fermions, on a 1D optical lattice consisting of two sublattices. Here, $\hat{\sigma}_\alpha^- = (\hat{\sigma}_\alpha^+)^{\dagger}$, where the $\hat{\sigma}_\alpha^{\pm}$ operators are related to the Pauli operators $\hat{\sigma}^{x,y,z}$ via the relations $\hat{\sigma}^x = (\hat{\sigma}^+ + \hat{\sigma}^-)$, $\hat{\sigma}^y = -i(\hat{\sigma}^+ - \hat{\sigma}^-)$, and $\hat{\sigma}^z = (2\hat{\sigma}^+ \hat{\sigma}^- - 1)$. One of the two sublattices in the fermionic model is constituted of the ‘‘odd’’ lattice sites, while the other contains the ‘‘even’’ ones. One of the two components of the fermions is situated on the odd sublattice, while the other is located on the even sublattice. The two components are distinguished by two different time-dependent chemical potentials $\mu_a(t)$ and $\mu_b(t)$, and the corresponding creation operators are denoted by \hat{a}^\dagger and \hat{b}^\dagger , respectively, following the usual fermionic anticommutation relations $\{\hat{f}_i, \hat{f}_j^\dagger\} = \delta_{i,j}$ and $\{\hat{f}_i, \hat{f}_j\} = \{\hat{f}_i^\dagger, \hat{f}_j^\dagger\} = 0$. Here, $\hat{f} = \hat{a}$ or \hat{b} , depending on whether i, j , the site indices, are odd or even, respectively.

Applying the transformation in Eq. (2), the form of the Hamiltonian representing the 1D two-component Fermi gas of spinless fermions at every time instant t , up to an additive constant energy $E_c(t) = [\mu_a(t) + \mu_b(t)]N/4$, can be written as

$$\hat{H} = \sum_{i=1}^{N/2} [\tau \{\hat{A}_i + \hat{B}_i + \gamma(\hat{C}_i + \hat{D}_i)\} + \mu_a(t)\hat{N}_i^a + \mu_b(t)\hat{N}_i^b], \quad (3)$$

where the operators $\hat{A}_i = \hat{a}_{2i-1}^\dagger \hat{b}_{2i} + \text{H.c.}$, $\hat{B}_i = \hat{b}_{2i}^\dagger \hat{a}_{2i+1} + \text{H.c.}$, $\hat{C}_i = \hat{a}_{2i-1}^\dagger \hat{b}_{2i}^\dagger + \text{H.c.}$, and $\hat{D}_i = \hat{b}_{2i}^\dagger \hat{a}_{2i+1}^\dagger + \text{H.c.}$ describe the interactions between the spinless fermions belonging to the odd and the even sublattices, with $\hat{N}_i^a = \hat{a}_{2i-1}^\dagger \hat{a}_{2i-1}$ and $\hat{N}_i^b = \hat{b}_{2i}^\dagger \hat{b}_{2i}$ being the corresponding number operators. Here, τ is the fermionic tunneling strength between a pair of even and odd sites, and N is the total number of lattice sites. Note that the existence of the two types of magnetic field (uniform and alternating) in the original model is reflected by the existence of the two sublattices in the fermionic model, differentiated by the chemical potentials and thereby leading to two types of fermionic operators, a and b .

B. Diagonalization

For general $\mu_{a,b}(t)$, the Hamiltonian given in Eq. (3) can be written as $\hat{H} = \sum_{p=1}^{N/4} \hat{H}_p$, with

$$\begin{aligned} \hat{H}_p = & J \cos \phi_p (\hat{a}_p^\dagger \hat{b}_p + a_{-p}^\dagger \hat{b}_{-p} + \hat{b}_p^\dagger \hat{a}_p + \hat{b}_{-p}^\dagger \hat{a}_{-p}) \\ & - iJ\gamma \sin \phi_p (\hat{a}_p^\dagger \hat{b}_{-p}^\dagger + \hat{a}_p \hat{b}_{-p} - \hat{a}_{-p}^\dagger \hat{b}_p^\dagger - \hat{a}_{-p} a_p) \\ & + h_+(t) (\hat{b}_p^\dagger \hat{b}_p + \hat{b}_{-p}^\dagger \hat{b}_{-p}) + h_-(t) (\hat{a}_p^\dagger \hat{a}_p + \hat{a}_{-p}^\dagger \hat{a}_{-p}) \\ & - 2h_1(t) \end{aligned} \quad (4)$$

via the Fourier transformations given by

$$\begin{aligned} \hat{a}_{2j+1}^\dagger &= \sqrt{\frac{2}{N}} \sum_{p=-N/4}^{N/4} \exp[i(2j+1)\phi_p] \hat{a}_p^\dagger, \\ \hat{b}_{2j}^\dagger &= \sqrt{\frac{2}{N}} \sum_{p=-N/4}^{N/4} \exp[i(2j)\phi_p] \hat{b}_p^\dagger, \end{aligned} \quad (5)$$

Here, $\phi_p = 2\pi p/N$, $h_\pm(t) = h_1(t) \pm h_2(t)$, and a_p^\dagger (b_p^\dagger) are fermionic operators. Since $[\hat{H}_p, \hat{H}_{p'}] = 0$, the above Fourier transformation decomposes the space upon which \hat{H} acts into noninteracting subspaces. These subspaces, each having a dimension 16, do not allow transitions within themselves, irrespective of the values of the system parameters J , γ , and $h_\pm(t)$. The diagonalization of the Hamiltonian \hat{H} is thereby reduced to the diagonalization of \hat{H}_p , acting on the p th subspace, which can be achieved by a convenient choice of the basis (see Appendix A). We note that the lowest eigenvalue of \hat{H}_p is given by $-\omega_+^4(p)$. The ground-state energy per site E_0 of the Hamiltonian can be obtained as $E_0 = -\frac{1}{2\pi} \int_0^{\pi/2} \omega_+^4(p) dp$.

C. Phases

We now briefly discuss the patterns of different phases, and the corresponding QPTs, present in the model described by the Hamiltonian in Eq. (3). We choose the strength of the transverse fields, uniform and alternating, as the tuning parameters. Information about the phase boundaries can be obtained from the second-order derivatives of the ground-state energy E_0 , with respect to λ_1 and λ_2 , where we take $\lambda_i = h_i/J$, $i = 1, 2$, and $h_{1(2)}(t = 0) = h_{1(2)}$. For $\gamma \neq 0$, the system undergoes two different second-order QPTs, namely, a transition from a paramagnetic (PM) to an antiferromagnetic (AFM) phase, and a transition from the AFM to a dimer (DM) phase. Figures 1(a) and 1(b) depict the spectrum of \hat{H}_p at critical points corresponding to AFM \leftrightarrow PM ($\lambda_1 = 1$, $\lambda_2 = 0$), and AFM \leftrightarrow DM ($\lambda_1 = 0$, $\lambda_2 = 0.8$) QPTs, respectively, for $\gamma = 0.8$ (see Appendix A for the expressions of the eigenvalues as functions of ϕ_p and the system parameters). Note that the vanishing of the energy gap in the spectrum occurs at $\phi_p = 0$ for the AFM \leftrightarrow PM transition, and at $\phi_p = \pm \frac{\pi}{2}$ for the AFM \leftrightarrow DM transition. On the other hand, Fig. 1(c) depicts the variation of the spectrum of \hat{H}_p as a function of ϕ_p for $\lambda_1 = 0.6$, $\lambda_2 = 0$. This point on the (λ_1, λ_2) plane belongs to the *factorization line*, which is discussed in Sec. IV B. One of our aims in this paper is to detect such transitions by using quantum information quantities. The phase boundaries corresponding to these transitions are given by the lines $\lambda_1^2 = \lambda_2^2 + 1$ and $\lambda_2^2 = \lambda_1^2 + \gamma^2$, respectively. It is interesting to note that there exists a set of duality relations, given by $\{h_1 \leftrightarrow h_2, J \leftrightarrow -\gamma\}$, by virtue of the unitary transformation $\{\hat{\sigma}_i^\alpha \rightarrow (-1)^i \hat{\sigma}_i^\alpha : \alpha = x, z\}$, which indicates that both AFM \leftrightarrow PM and AFM \leftrightarrow DM transitions belong to the same universality class, namely, the Ising universality class [18]. One must also note that for $h_2 = 0$, the model reduces to the well-known anisotropic XY model in a uniform transverse magnetic field of magnitude h_1 .

III. CANONICAL-EQUILIBRIUM AND TIME-EVOLVED STATES: LOCAL DENSITY MATRICES

In this paper, we intend to study the statistical mechanical properties of the model in terms of bipartite quantum correlations. We now briefly introduce the notions of canonical equilibrium states and time-evolved states corresponding to the Hamiltonian given in Eq. (1), and describe how two-spin reduced density matrices corresponding to such states can be

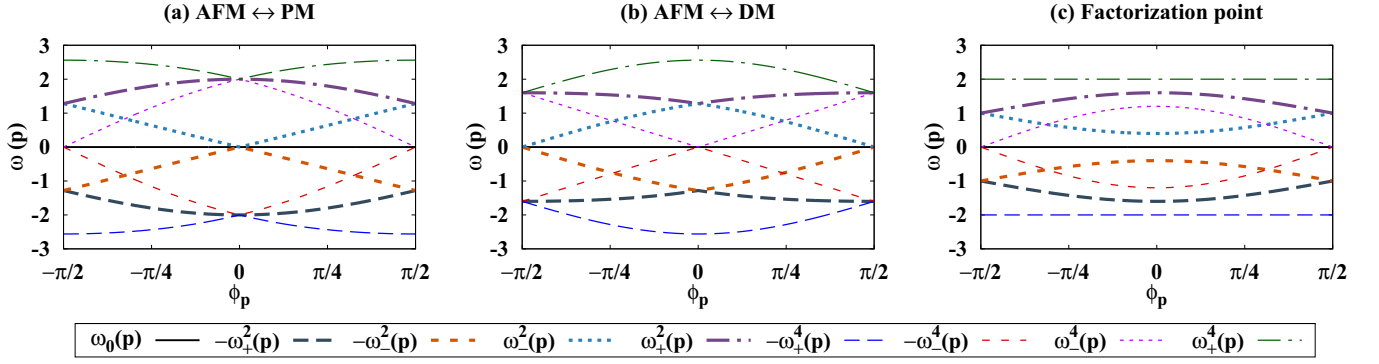


FIG. 1. Spectrum of \hat{H}_p for $\gamma = 0.8$. (a), (b) Variation of the eigenvalues of \hat{H}_p as a function of ϕ_p at the AFM \leftrightarrow PM ($\lambda_1 = 1$, $\lambda_2 = 0$) and the AFM \leftrightarrow DM ($\lambda_1 = 0$, $\lambda_2 = 0.8$) transitions. (c) Patterns of the eigenvalues of \hat{H}_p against ϕ_p at the factorization point (see Sec. IV B). The chosen parameter values for the factorization point are $\lambda_1 = 0.6$, $\lambda_2 = 0$. The minimum eigenvalue in all the cases is $-\omega_+^4(p)$ (given in Appendix A). The energy gap vanishes at $\phi_p = 0$ for the AFM \leftrightarrow PM and at $\phi_p = \pm \frac{\pi}{2}$ for the AFM \leftrightarrow DM QPT point.

obtained. For our purpose, we consider the situation where the time-dependent magnetic fields $h_1(t)$ and $h_2(t)$ are chosen as

$$h_1(t) = \begin{cases} h_1, & t \leq 0 \\ 0, & t > 0 \end{cases}, \quad h_2(t) = \begin{cases} h_2, & t \leq 0 \\ 0, & t > 0 \end{cases}. \quad (6)$$

The canonical equilibrium state (CES) of the system at time t is given by

$$\hat{\rho}_{eq}(t) = \frac{e^{-\beta \hat{H}(t)}}{Z}, \quad (7)$$

where $Z = \text{Tr}\{\exp[-\beta \hat{H}(t)]\}$ is the partition function, and $\hat{H}(t)$ is given in Eq. (1). Here, $\beta = 1/k_B T$, T is the absolute temperature, and k_B is the Boltzmann constant. In all our calculations, we set $k_B = 1$. For the purpose of this paper, we consider a system which is in contact with a heat bath at temperature T for a long time up to the instant that we call $t = 0$, so that a thermal equilibrium between the system and the heat bath have developed. The equilibrium is in the canonical sense, allowing exchange of energy between the bath and the system with the usual average energy constraint, but forbidding exchange of particle. To study quantum correlations in the evolution, we choose the canonical equilibrium state $[\hat{\rho}_{eq}(t = 0)]$ as an initial state. When the magnetic fields are switched off, the CES starts evolving in time following the Schrödinger equation dictated by the Hamiltonian in Eq. (1). At any time t , the time-evolved state (TES) $\hat{\rho}(t)$ is given by

$$\hat{\rho}(t) = e^{-i\hat{H}t} \hat{\rho}_{eq}(t = 0) e^{i\hat{H}t}, \quad (8)$$

where \hat{H} represents the Hamiltonian given in Eq. (1) at $t > 0$.

A. Local density matrices

To investigate the behavior of bipartite quantum correlation measures of the CES and TES, computation of the single-site and the two-site reduced density matrices of the entire state is necessary. Since we consider the system with periodic boundary condition, all the nearest-neighbor bipartite states are the same and hence their two-spin correlation functions would be independent of the choice of the pairs of spins, while the single-site magnetizations depend on whether the lattice site is even or odd. A general single-site density matrix, given

by $\hat{\rho}^i = [\mathbb{I} + \sum_{\alpha=x,y,z} m^\alpha(t) \hat{\sigma}_i^\alpha]/2$, can be obtained by tracing out all the spins except the spin at the lattice site α , which is ‘‘o’’ for the odd site and ‘‘e’’ for the even site. Here, \mathbb{I} is the identity operator in the qubit Hilbert space. For CES corresponding to a real Hamiltonian, $\hat{\rho}_{eq}^{i*}(t) = \hat{\rho}_{eq}^i(t)$, implying $m_i^y(t) = 0$ with the complex conjugation being taken in the computational basis. Also, the Hamiltonian possesses a global phase-flip symmetry, such that $[H, \Pi_i \sigma_i^z] = 0$, implying $m_i^x(t) = 0$. Hence, the single-site reduced density matrix corresponding to the CES is given by $\hat{\rho}_{eq}^i(t) = [\mathbb{I} + m_i^z(t) \hat{\sigma}_i^z]/2$. On the other hand, $\hat{\rho}^i(t)$ corresponding to the evolved state is not necessarily equal to its complex conjugation, and the existence of the global phase-flip symmetry is a complicated issue due to the time dependence of the Hamiltonian. However, use of the Wick’s theorem leads to the same form of $\hat{\rho}^i(t)$, when TES is considered instead of the CES.

Let us now consider the two-site reduced density matrix $\hat{\rho}_{ij}$, corresponding to the spins at the lattice sites i and j , and obtained by tracing out all the other spins except those at the positions i and j . In the present case, we restrict ourselves to nearest-neighbor pairs of spins, such that $j \equiv i + 1$. To keep the notations uncluttered, from now on, we shall discard the lattice indices, and denote the nearest-neighbor two-spin density matrix by $\hat{\rho}_{eo}$, where we assume that the lattice site i belongs to the even sublattice without any loss of generality. The two-party state $\hat{\rho}_{eo}$, of the CES and TES in this system, can be written as

$$\hat{\rho}_{eo} = \frac{1}{4} \left[\mathbb{I}_e \otimes \mathbb{I}_o + m_e^z \hat{\sigma}_e^z \otimes \mathbb{I}_o + \mathbb{I}_e \otimes m_o^z \hat{\sigma}_o^z + \sum_{\alpha, \beta=x,y,z} c_{eo}^{\alpha\beta} \hat{\sigma}_e^\alpha \otimes \hat{\sigma}_o^\beta \right], \quad (9)$$

where $c_{eo}^{\alpha\beta} = \text{Tr}[\hat{\sigma}_e^\alpha \otimes \hat{\sigma}_o^\beta \hat{\rho}_{eo}]$ are the two-site spin correlation tensor. In the case of CES, by using arguments similar to those in the case of the single-site density matrix, and by applying the Wick’s theorem, one can show that only diagonal elements of the correlation tensor, given by $c_{eo}^{\alpha\alpha}$, $\alpha = x, y, z$, remain. On the other hand, in the case of TES, c_{eo}^{xy} and c_{eo}^{yx}

remain nonzero in addition to the diagonal correlators. For brevity, from now onward, we discard the site indices while mentioning the two-spin correlators.

B. Quantum correlations between two modes of a 1D Fermi gas

We now demonstrate that the quantum correlation between a nearest-neighbor spin pair chosen from the anisotropic XY model in a uniform and an alternating transverse magnetic field is the same as that present between two fermionic modes located at the two nearest-neighbor lattice sites in the fermionic model given in Eq. (3). Without any loss of generality, the two-site density matrix of a nearest-neighbor pair of lattice sites, denoted by “ eo ,” can be written as $\hat{\rho}_{eo}^f = \frac{1}{4} \sum_{k,l} \xi_{kl} \hat{\zeta}_e^k \hat{\zeta}_o^l$, where $k, l = 0, 1, 2, 3$, and $\hat{\zeta}_\alpha = \{\mathbb{I}, (c_\alpha + c_\alpha^\dagger), -i(c_\alpha - c_\alpha^\dagger), (2c_\alpha^\dagger c_\alpha - 1)\}$. Here, $c \equiv a(b)$ depending on whether $\alpha \equiv o(e)$. The coefficients $\{\xi_{kl}\}$ are given by $\xi_{kl} = \text{tr}[\hat{\rho}_{eo}^f (\hat{\zeta}_e^k \hat{\zeta}_o^l)^\dagger]$. Expanding and applying Wick’s theorem as in Sec. III A, the TES corresponding to a pair of fermionic modes on the “ eo ” site pair for the fermionic model is given by

$$\hat{\rho}_{eo}^f = \frac{1}{4} [\mathbb{I}_{4 \times 4} + \xi_{03} \hat{\zeta}_o^3 + \xi_{30} \hat{\zeta}_e^3 + \xi_{11} \hat{\zeta}_e^1 \hat{\zeta}_o^1 + \xi_{22} \hat{\zeta}_e^2 \hat{\zeta}_o^2 + \xi_{33} \hat{\zeta}_e^3 \hat{\zeta}_o^3 + \xi_{12} \hat{\zeta}_e^1 \hat{\zeta}_o^2 + \xi_{21} \hat{\zeta}_e^2 \hat{\zeta}_o^1]. \quad (10)$$

With a convenient choice of basis given by $\{|0\rangle, \hat{a}^\dagger|0\rangle, \hat{b}^\dagger|0\rangle, \hat{b}^\dagger \hat{a}^\dagger|0\rangle\}$, where $|0\rangle$ represents the vacuum state, the individual terms in Eq. (10) can be expressed in their respective matrix forms. A comparison with the matrix forms of the operators $\sigma_e^\alpha \otimes \sigma_o^\beta$ implies that in matrix form, $\hat{\rho}_{eo}^f$ can be expressed as

$$\hat{\rho}_{eo}^f = \frac{1}{4} \left[\mathbb{I}_e \otimes \mathbb{I}_o - m_e^z \sigma_e^z \otimes \mathbb{I}_o - \mathbb{I}_e \otimes m_o^z \sigma_o^z - c_{eo}^{xy} \sigma_e^x \otimes \sigma_o^y - c_{eo}^{yx} \sigma_e^y \otimes \sigma_o^x + \sum_{\alpha=x,y,z} c_{eo}^{\alpha\alpha} \sigma_e^\alpha \otimes \sigma_o^\alpha \right]. \quad (11)$$

Here, σ^α are 2×2 the Pauli matrices, where, e.g., $\sigma_z^e = \begin{pmatrix} 1 & 0 \\ 0 & -1 \end{pmatrix}$ in the $\{|0\rangle, \hat{b}^\dagger|0\rangle\}$ basis and where, e.g., $\sigma_y^o = \begin{pmatrix} 0 & -i \\ i & 0 \end{pmatrix}$ in the $\{|0\rangle, \hat{a}^\dagger|0\rangle\}$ basis. Note that $\hat{\rho}_{eo}^f$ is connected to the TES $\hat{\rho}_{eo}$ in the spin model via a local unitary transformation given by $\hat{\rho}_{eo}^f = (\sigma^x \otimes \sigma^x) \hat{\rho}_{eo} (\sigma^x \otimes \sigma^x)$, thereby implying no change in the values of the chosen measure of bipartite quantum correlation.

IV. STATIC BEHAVIOR OF QUANTUM CORRELATIONS

In this section, we discuss the behavior of bipartite quantum correlation measures of the reduced density matrix of the nearest-neighbor qubit pair, obtained from the zero temperature and the thermal states of the model. Since the model is not evolving, we call the states as static states. For our purpose, we consider logarithmic negativity (LN), denoted by $\mathcal{L}(\rho_{AB})$, and quantum discord (QD), denoted by $\mathcal{D}(\rho_{AB})$, in the ground and thermal states of the model. The former belongs to the entanglement separability paradigm, while the latter is from the quantum information-theoretic regime of quantum correlations. Short descriptions of these measures are provided in Appendix B. While computing QD

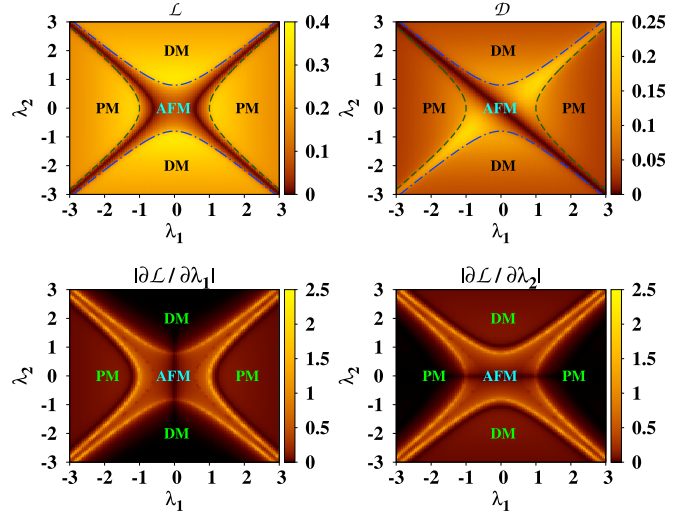


FIG. 2. (Top horizontal panels) Variations of LN (left panel) and QD (right panel) as functions of the transverse magnetic field λ_1 and the alternating field λ_2 in the thermodynamic limit at $\beta \rightarrow \infty$ and $\gamma = 0.8$. The phase boundaries $\lambda_1^2 = \lambda_2^2 + 1$ (PM \leftrightarrow AFM) and $\lambda_2^2 = \lambda_1^2 + \gamma^2$ (AFM \leftrightarrow DM) are represented by the dashed and dotted-dashed lines, respectively, while the different shades in the figures represent different values of quantum correlations. (Bottom horizontal panels) Variations of the first derivative of LN with respect to λ_1 (left panel) and the same quantity of LN with respect to λ_2 (right panel) with $N \rightarrow \infty$ at $\beta \rightarrow \infty$, and $\gamma = 0.8$. The value of the respective first derivatives of LN diverges at the phase boundaries $\lambda_1^2 = \lambda_2^2 + 1$ (PM \leftrightarrow AFM) and $\lambda_2^2 = \lambda_1^2 + \gamma^2$ (AFM \leftrightarrow DM). Different shades in the figures represent different values of the first derivative of LN with respect to respective parameter. All the quantities plotted in all the figures are dimensionless, except LN which is in ebits and QD in bits.

in the entire paper, we always perform local rank-1 projection measurement on the “even” qubit. We choose two different types of quantum correlation quantities since they behave differently as demonstrated in the XY as well as the XXZ model [21,23,24].

A. Quantum correlations at zero temperature

In the limit $\beta \rightarrow \infty$, we now investigate the behavior of LN and QD, as functions of the system parameters λ_1 and λ_2 , in the thermodynamic limit. For this system, m_z^e, m_z^o and all the nonzero classical correlations can be obtained analytically by diagonalizing \hat{H}_p , following the similar prescription for the XY model (see Appendix C) and hence the exact computation of LN and QD is possible, as depicted in the top horizontal panels of Fig. 2. To keep the notation uncluttered, from now on, we denote LN by \mathcal{L} and QD by \mathcal{D} . In this paper, all the analyses are carried out for $\gamma = 0.8$ unless specified otherwise. The qualitative feature of the entire investigation remains the same for $\gamma \neq 0$. Note that the LN has a high value in the DM and PM phases, while the value is low in the AFM phase. On the other hand, the value of QD is moderate in the PM region. In the AFM region, the QD has a low value except in the cases where the values of λ_1 and λ_2 are comparable. Along the line $\lambda_1 = -\lambda_2$, QD is vanishingly small. Note that the situation is reversed if one performs measurement on the odd qubit while determining QD. In that case, low values of QD are found

along the $\lambda_1 = \lambda_2$ line. Hence, the asymmetry imposed into the model due to the introduction of the alternating field is captured from the distribution of QD values over the AFM region in the parameter space of (λ_1, λ_2) , but not by LN. However, in the case of LN, there exist two zero-entanglement lines in the AFM phase, as depicted in the left panel of the top horizontal row of Fig. 2, which represent fully separable ground states. These lines, which we refer to as the ‘‘factorization lines,’’ are discussed in detail in the subsequent section.

One must note here that the introduction of only a local parameter, i.e., the alternating transverse field, in the well-known transverse-field XY Hamiltonian [30,31], gives rise to the DM phase, which is not present in the transverse-field XY model. It is interesting to investigate how the QPTs occurring at the AFM \leftrightarrow DM phase boundaries can be characterized using entanglement and information-theoretic quantum correlation measures, and whether such characteristic behaviors are similar to those observed in the case of the AFM \leftrightarrow PM transition in this model as well as in the usual transverse-field XY model [30,31]. In the thermodynamic limit, and for the latter case, the QPT is found to be signaled by a divergence in the first derivative of entanglement as well as in the information-theoretic measures with respect to the system parameters λ_1 and λ_2 (see the bottom panel of Fig. 2). We find that, similar to the AFM \leftrightarrow PM QPT, other transitions can also be detected by the first derivative of appropriate measures of quantum correlations. As an example, in Fig. 2 (bottom horizontal panels), we plot $|\partial\mathcal{L}/\partial\lambda_1|$ (left panel) and $|\partial\mathcal{L}/\partial\lambda_2|$ (right panel) as functions of λ_1 and λ_2 for $\gamma = 0.8$, $\beta \rightarrow \infty$, and $N \rightarrow \infty$. From the figures, we can clearly see that both $|\partial\mathcal{L}/\partial\lambda_1|$ (left panel) and $|\partial\mathcal{L}/\partial\lambda_2|$ (right panel) diverge at the AFM \leftrightarrow DM and AFM \leftrightarrow PM boundaries. We plot the absolute values of the first derivatives of LN for a better representation of the divergence, as the actual first derivative can tend to both positive as well as negative infinity, depending on the variation of LN with respect to λ_1 and λ_2 . Note here that there exist two lines, one vertical ($|\partial\mathcal{L}/\partial\lambda_1|$) and the other horizontal ($|\partial\mathcal{L}/\partial\lambda_2|$) in the variations of the first derivative of LN, as depicted in Fig. 2, over which the value of LN remains almost constant. This is indicated by the low value of the first derivative of LN over those lines. Note also that there exist several models in which bipartite entanglement cannot detect quantum phase transitions [1,2,55]. Such example includes the spin liquid-dimer transition in 1D J_1 - J_2 model [56]. The results obtained here show that this is not the case for the XY model with uniform and alternating transverse field.

1. Finite-size scaling analysis

Advancement of experimental techniques has made the laboratory realization of several quantum many-body systems of finite size, such as the quantum anisotropic XY model with a transverse alternating magnetic field, possible [8,9], which highlights the importance of studying the behavior of quantum correlations in the context of QPTs in system of finite number of spins. Towards this aim, we present the finite-size scaling analysis of the system using the bipartite quantum correlations, and determine the scaling exponents. More specifically, we discuss the finite-size scaling of the

system at the QPTs corresponding to (i) AFM \leftrightarrow PM and (ii) AFM \leftrightarrow DM transitions.

(i) AFM \leftrightarrow PM transitions: At $\lambda_2 = 0$, the model reduces to the widely studied anisotropic XY model in a uniform transverse magnetic field of strength λ_1 . As $N \rightarrow \infty$ and $\beta \rightarrow \infty$, the model undergoes a QPT, between the quantum PM phase and the AFM phase, at $\lambda_1^c = \pm 1$. It is well known that this QPT is signaled by a nonanalyticity in the first derivatives of the quantum correlation measures \mathcal{Q} with respect to the system parameter λ_1 [21,23]. With the introduction of the transverse alternating field λ_2 , the QPT point changes according to the line $\lambda_1^2 = \lambda_2^2 + 1$, which denotes the phase boundary between the AFM and the quantum PM phase in the present model. As shown in Fig. 2, the AFM \leftrightarrow PM transition is also signaled by a nonanalyticity in the first derivative of LN or QD, with respect to λ_1 (λ_2), when λ_2 (λ_1) is kept fixed as $N \rightarrow \infty$. In the case of a system of finite size, the QPT is signaled by a maximum or a minimum in the variation of the first derivative of LN and QD with respect to λ_1 (λ_2), for fixed values of λ_2 (λ_1) (see Fig. 3). The position of the maximum or minimum denotes the position of the critical point on the axes of the respective system parameter. The maximum or minimum sharpens with increasing system size, and the position of the QPT approaches the QPT point as $N \rightarrow \infty$, denoted by $\lambda_{1(2)}^c(\infty)$, as

$$\lambda_{1(2)}^c(N) = \lambda_{1(2)}^c(\infty) + \alpha_{1(2)} N^{-\nu_{1(2)}}. \quad (12)$$

Here, $\alpha_{1(2)}$ are dimensionless constants, and $\nu_{1(2)}$ are the scaling exponents.

Figure 3(a) depicts the variation of derivative of LN and QD, as functions of λ_1 , as $\beta \rightarrow \infty$, for fixed value of λ_2 i.e., $\lambda_2 = 1.5$ with $\gamma = 0.8$. The approach of the QPT points $\lambda_1^c(N)$ at finite N , towards the QPT point in the thermodynamic limit $\lambda_1^c(\infty)$, are depicted in the insets. Fitting the numerical data with Eq. (12), one can estimate the values of α_1 and ν_1 . Table I(a) contains the values of $\alpha_{1,2}$ and $\nu_{1,2}$, in the case of both LN and QD, when the value of λ_2 (λ_1) is kept fixed at $\lambda_2 = 0$ and 1.5 ($\lambda_1 = 1.5$). Note that the values of $\alpha_{1,2}$ and $\nu_{1,2}$ change with γ although the qualitative feature remains invariant.

(ii) AFM \leftrightarrow DM transition: Similar to the case of AFM \leftrightarrow PM transition, in the thermodynamic limit, the AFM \leftrightarrow DM transition is signaled by a nonanalyticity in the first derivative of LN or QD, with respect to either of λ_1 and λ_2 . It is interesting to investigate how the position of the QPT point, as determined by the position of the sharp peak in the variation of the derivatives of LN and QD with respect to either λ_1 or λ_2 , changes with a variation in the system size. In order to do so, one may try to determine the canonical equilibrium state at zero temperature by using the same methodology as in the case of the AFM \leftrightarrow PM transition. However, due to the approximations involved in determining the zero-temperature state, in the present case, LN and QD, as functions of either of λ_1 and λ_2 , exhibit finite jumps in values at the QPT point, thereby forbidding a finite-size analysis in a similar fashion as in the previous case (for a discussion on the behavior of the finite jumps, and a figure, see Appendix E). Therefore, we employ the exact diagonalization technique in the present case, and determine

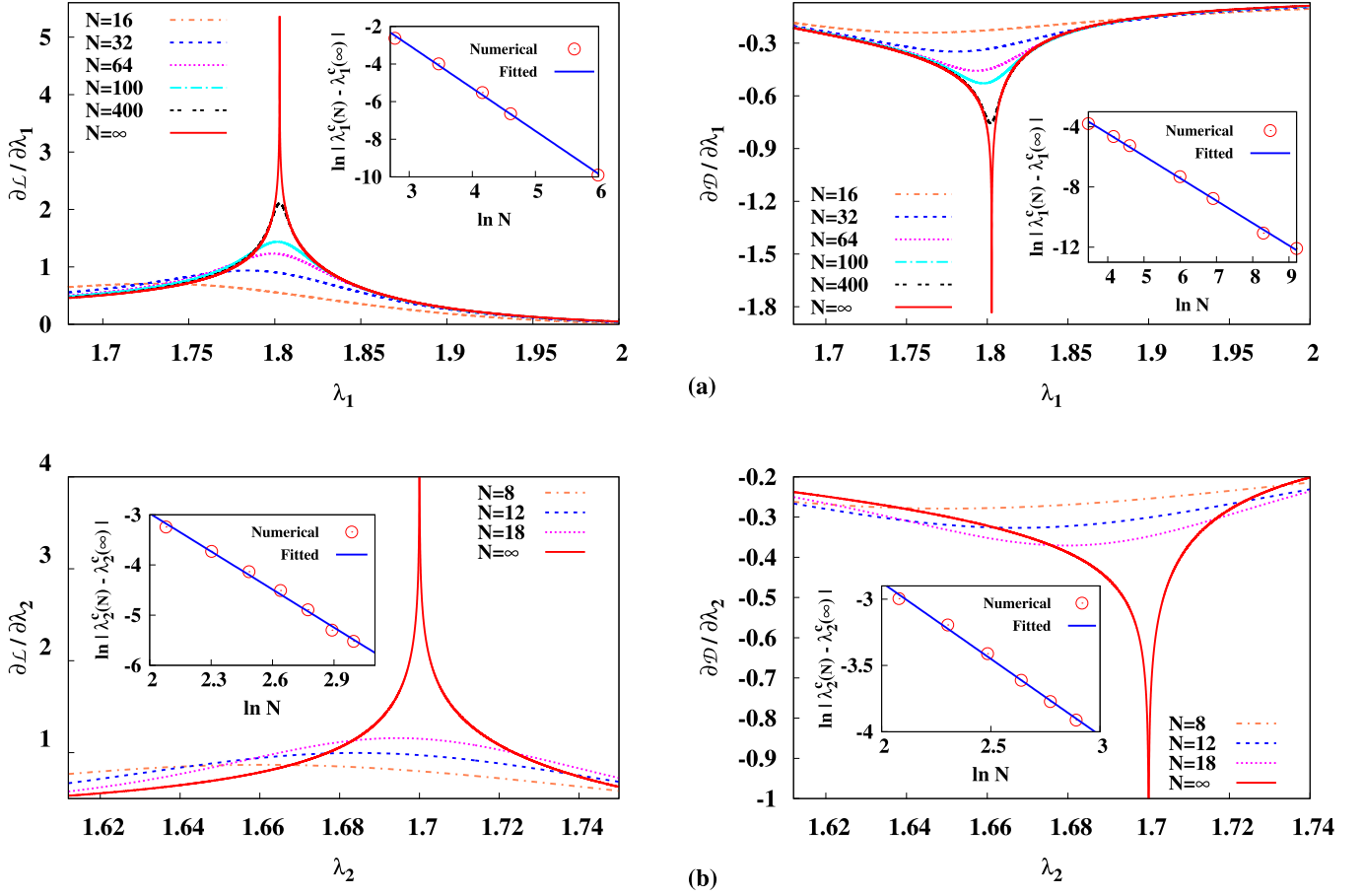


FIG. 3. Finite-size scaling using LN and QD in (a) AFM \leftrightarrow PM and (b) AFM \leftrightarrow DM phase transitions. (a) The figure in the left (right) panel depicts the variation of $\partial\mathcal{L}/\partial\lambda_1$ ($\partial D/\partial\lambda_1$) with λ_1 across the AFM \leftrightarrow PM QPT for different values of N , with $\lambda_2 = 1.5$ and $\gamma = 0.8$. (Insets) Corresponding variations of $\ln|\lambda_1^c(N) - \lambda_1^c(\infty)|$ (both numerical data and fitted line) as a function of $\ln N$. (b) The figure in the left (right) panel depicts the variation of LN (QD) with λ_2 across the AFM \leftrightarrow DM QPT for different values of N , with $\lambda_1 = 1.5$. (Insets) Corresponding variations of $\ln|\lambda_2^c(N) - \lambda_2^c(\infty)|$ (both numerical data and fitted line) as a function of $\ln N$. All the quantities plotted are dimensionless, except LN which is in ebits and QD which is in bits.

the nondegenerate ground state of the Hamiltonian given in Eq. (1) by using Lanczos algorithm [57]. The reduced density matrix corresponding to a nearest-neighbor even-odd spin pair, labeled by “ eo ,” can be determined by tracing out all

TABLE I. Finite-size scaling exponents and fitting parameters for the QPT corresponding to AFM \leftrightarrow PM transition. For all the computations, $\gamma = 0.8$.

Tuning parameter: λ_1		
λ_2	LN	QD
0.0	$\nu_1 = 1.645 \pm 0.013$ $\ln \alpha_1 = 2.842 \pm 0.070$	$\nu_1 = 1.292 \pm 0.093$ $\ln \alpha_1 = 1.851 \pm 0.631$
1.5	$\nu_1 = 2.278 \pm 0.053$ $\ln \alpha_1 = 3.828 \pm 0.230$	$\nu_1 = 1.489 \pm 0.027$ $\ln \alpha_1 = 1.507 \pm 0.175$
Tuning parameter: λ_2		
λ_1	LN	QD
1.5	$\nu_2 = 1.941 \pm 0.042$ $\ln \alpha_2 = 3.614 \pm 0.204$	$\nu_2 = 1.507 \pm 0.008$ $\ln \alpha_2 = 2.380 \pm 0.052$

the other spin variables from the ground state. Using the reduced density matrix, the nearest-neighbor LN and QD can be computed. Here, for the purpose of discussions, the first derivatives of LN and QD, with respect to λ_2 , by keeping λ_1 fixed at 1.5, are plotted in Fig. 3(b). We find that in the case of the AFM \leftrightarrow DM transition also, the position of the QPT at a finite N approaches the actual QPT point at $N \rightarrow \infty$ according to an equation similar to Eq. (12), where the constants are denoted by $\alpha_{1,2}$ and $\nu_{1,2}$. For example, for $\lambda_1 = 1.5$, the corresponding values of these fitting parameters are $\nu_2 = 2.525 \pm 0.084$, $\ln \alpha_2 = 2.077 \pm 0.220$ (for LN), and $\nu_2 = 1.153 \pm 0.036$, $\ln \alpha_2 = -0.568 \pm 0.092$ (for QD).

B. Factorization line: Separable ground state

We now discuss the occurrence of the separable ground state in the AFM phase of the model which can be observed by considering the variation of bipartite as well as multipartite entanglement as functions of λ_1 and λ_2 (Fig. 2). The symmetry of the Hamiltonian [Eq. (1)] under PBC motivates one to look

for a separable eigenstate of the form

$$|\psi\rangle = \prod_{i=0}^{\frac{N}{2}-1} |\psi_{2i+1}^o\rangle \otimes |\psi_{2i+2}^e\rangle, \quad (13)$$

having a Néel-type order, where $|\psi_{\alpha}^{o(e)}\rangle$ are the states of the spins on the odd (even) site α . The Hamiltonian can be written as $H = \sum_{i=0}^{(N/2)-1} (H_{2i+1,2i+2}^{oe} + H_{2i+2,2i+3}^{eo})$, where H^{oe} is the two-site Hamiltonian given by

$$H^{eo} = J \left\{ \frac{1+\gamma}{4} \sigma_e^x \sigma_o^x + \frac{1-\gamma}{4} \sigma_e^y \sigma_o^y \right\} + \frac{h_+}{2} \sigma_e^z + \frac{h_-}{2} \sigma_o^z, \quad (14)$$

with $h_{\pm} = h_1 \pm h_2$, defined on an even-odd pair of sites, and H^{oe} can be obtained from H^{eo} straightforwardly by interchanging the site indices. Using Eq. (13), the lowest separable eigenenergy can be obtained as

$$\begin{aligned} E_{\min}^{\text{sep}} &= \min_{|\psi^e\rangle, |\psi^o\rangle} \langle \psi | H | \psi \rangle \\ &= \sum_{i=0}^{\frac{N}{2}-1} \min_{|\psi^e\rangle, |\psi^o\rangle} \langle \psi^e | \langle \psi^o | H_{2i+1,2i+2}^{eo} | \psi^e \rangle | \psi^o \rangle \\ &\quad + \sum_{i=0}^{\frac{N}{2}-1} \min_{|\psi^o\rangle, |\psi^e\rangle} \langle \psi^o | \langle \psi^e | H_{2i+2,2i+3}^{oe} | \psi^o \rangle | \psi^e \rangle \\ &= N \min_{|\psi^e\rangle, |\psi^o\rangle} \langle \psi^e | \langle \psi^o | H^{eo} | \psi^e \rangle | \psi^o \rangle, \end{aligned}$$

where we have used the fact that H^{eo} and H^{oe} are energetically equivalent. This leads to a minimum separable energy per site ϵ , given by $\epsilon = \min_{|\psi^e\rangle, |\psi^o\rangle} \langle \psi^e | \langle \psi^o | H^{eo} | \psi^e \rangle | \psi^o \rangle$. Without any

loss of generality, one can choose the states $|\psi^{e(o)}\rangle$ to be

$$|\psi^{e(o)}\rangle = \cos \frac{\theta_{e(o)}}{2} |0\rangle + \exp i \phi_{e(o)} \sin \frac{\theta_{e(o)}}{2} |1\rangle, \quad (15)$$

where $\theta_{e(o)}$ and $\phi_{e(o)}$ are real parameters such that $0 \leq \theta_{e(o)} \leq \pi$ and $0 \leq \phi_{e(o)} \leq 2\pi$. The two-spin reduced density matrix ρ_{eo} , corresponding to the odd-even pair of spins, is then given by $\rho_{eo} = \rho_e \otimes \rho_o$, where $\rho_{e(o)} = |\psi^{e(o)}\rangle \langle \psi^{e(o)}|$. Since the Hamiltonian in Eq. (1) is a real one, we expect $\rho_{eo} = \rho_{eo}^*$, leading to

$$\epsilon = \min_{\theta_e, \theta_o} \frac{1}{4} \left\{ J(1+\gamma) \sin \theta_e \sin \theta_o + h_+ \cos \theta_e + h_- \cos \theta_o \right\}, \quad (16)$$

where the optimization over the states $|\psi^{e(o)}\rangle$ is reduced to an optimization over the real parameter space of θ_o and θ_e . The minimum is achieved for

$$\begin{aligned} \theta_e &= \tan^{-1} \left\{ \pm \frac{1}{h_+} \sqrt{\frac{J^4(1+\gamma)^4 - h_+^2 h_-^2}{J^2(1+\gamma)^2 + h_+^2}} \right\}, \\ \theta_o &= \tan^{-1} \left\{ \pm \frac{1}{h_-} \sqrt{\frac{J^4(1+\gamma)^4 - h_+^2 h_-^2}{J^2(1+\gamma)^2 + h_-^2}} \right\}. \end{aligned} \quad (17)$$

However, the state $|\psi\rangle$ [Eq. (13)] would be the ground state of the Hamiltonian if $\epsilon = \epsilon_0$, the ground-state energy of the two-spin Hamiltonian H^{eo} [44,45]. We find that the ground

state of H^{eo} is nondegenerate, with a ground-state energy given by $\epsilon_0 = \frac{1}{2} \sqrt{J^2 + 4h_2^2}$. Determination of ϵ using the values of $\theta_{e(o)}$, and equating to ϵ_0 , leads to the following condition:

$$h_1^2 = h_2^2 + J^2(1-\gamma^2), \quad (18)$$

equivalently $\lambda_1^2 = \lambda_2^2 + (1-\gamma^2)$, which represents a line on the (λ_1, λ_2) plane for fixed values of γ . The ground state of the Hamiltonian, at every point on this line on the (λ_1, λ_2) plane, is separable, represented by a line of vanishing entanglement (Fig. 2). We call this line as *factorization line*. At any point on this line, the minimum eigenvalue of \hat{H}_p , given by $-\omega_+^4(p)$, becomes independent of ϕ_p , as demonstrated for $(\lambda_1 = 0.6, \lambda_2 = 0)$ with $\gamma = 0.8$ in Fig. 1(c). This feature is in contrast to the ϕ_p dependence of $-\omega_+^4(p)$ at the QPT points [see Figs. 1(a) and 1(b)].

C. Effect of temperature on quantum correlations

Quantum correlations are known to be fragile quantities, and are expected to decay with increasing thermal noise in the system. Moreover, absolute zero temperature is hard to be achieved in a real experiment. It is therefore interesting to investigate the effect of thermal fluctuations on the bipartite quantum correlations corresponding to the Hamiltonian [Eq. (1)]. The patterns of LN and QD as functions of λ_1 and λ_2 , for $\beta J = 5$ [Fig. 4(a)] and $\beta J = 2$ [Fig. 4(b)] are plotted in Fig. 4. In the case of LN, we observe that starting from the factorization line at $\beta \rightarrow \infty$, a zero-entanglement region grows with increasing temperature, and spans the entire AFM phase at sufficiently high temperature. Note here that the zero-entanglement region at $\beta J > 0$ can also be found in the PM phase, while it is absent in the DM phase even at high

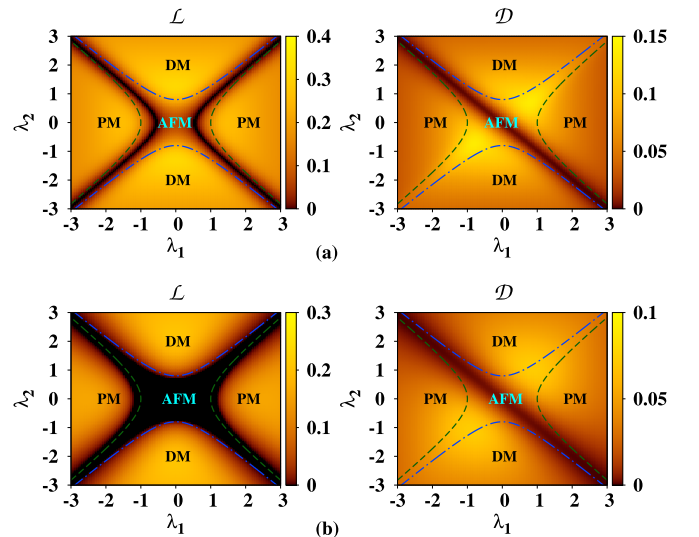


FIG. 4. Variation of LN and QD as functions of the transverse magnetic field h_1 and the alternating field h_2 in the thermodynamic limit at (a) $\beta J = 5$ and (b) $\beta J = 2$, and $\gamma = 0.8$. The zero-temperature phase boundaries $\lambda_1^2 = \lambda_2^2 + 1$ (PM \leftrightarrow AFM) and $\lambda_2^2 = \lambda_1^2 + \gamma^2$ (AFM \leftrightarrow DM) are also plotted for comparison, represented by the dashed and dotted-dashed lines, respectively. All the quantities plotted are dimensionless, except LN and QD, which are in ebits and bits, respectively.

temperature. A few interesting features emerge from these results.

(i) The rate of spreading of the vanishing entanglement region with increasing temperature is found to be much slower towards the PM phase compared to that inside the AFM phase. This can be easily perceived from the fact that with the increase of temperature from $\beta J = 5$ to 2, the entanglement vanishes in the entire AFM phase, but covers only a small region in the PM phase. It implies that bipartite entanglement is more fragile in the AFM region compared to the other phases.

(ii) Remarkably, bipartite entanglement in the DM phase is the most robust against increasing thermal noise among the three phases.

(iii) The effect of thermal noise on QD is less drastic compared to that in the case of LN, as observed from Fig. 4. With increasing temperature, the minimum value of QD along the line $\lambda_1 = -\lambda_2$ increases. However, the qualitative distribution of QD over the (λ_1, λ_2) plane remains unchanged.

Remark 1. We choose $\beta J = 2.0$ and treat as high temperature since bipartite entanglement of the AFM phase has been destroyed at this temperature. However, if one increases temperature beyond $\beta J = 2$, LN in the entire region of (λ_1, λ_2) plane becomes zero.

Remark 2. For the purpose of demonstration, we have kept the anisotropy parameter constant to a fixed value $\gamma = 0.8$. One must remember that the definition of “high” βJ depends, along with the other system parameters, on the anisotropy parameter also. However, the qualitative features, such as the robustness of bipartite entanglement in the DM phase compared to other phases, or the fragility of LN in the AFM phase remain unchanged with a change in the value of the anisotropy parameter.

1. Monotonicity versus nonmonotonicity

Up to now we have discussed the variation in the pattern of entanglement and QD with the increase of temperature. We now report the existence of nonmonotonic variation of LN and QD as functions of temperature in this model. Such nonmonotonicity is known for other quantum many-body Hamiltonians, including the transverse-field XY model [25–27]. Since the model under consideration possesses a different phase diagram than the XY model, nonmonotonicity of quantum correlations, especially entanglement with temperature, may reveal some additional feature. We will show that this is indeed the case. For fixed choices of (λ_1, λ_2) , typical variation profiles exhibiting nonmonotonicity of LN and QD with temperature, as shown in Fig 5. The importance of nonmonotonic behavior of bipartite quantum correlation lies in the fact that even at high temperature, which is much easier to attain in the laboratory, a higher value of quantum correlations is obtained compared to the state with lower temperature. This has potential applicability in the realization of those quantum protocols in the laboratory, which use quantum correlations as resources.

It is therefore necessary to map the occurrence of nonmonotonic variations of bipartite quantum correlations over the phase plane of the model, so that the useful regions at finite temperature can be recognized. Let us consider a set of values in the space of the system parameters, denoted by

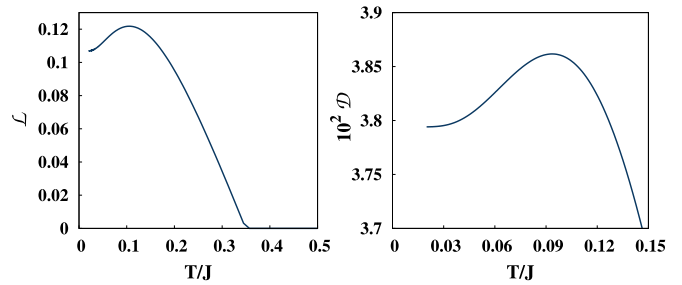


FIG. 5. Nonmonotonic variations of LN (left panel) and QD (right panel) with temperature. We choose $\lambda_1 = -0.9$, $\lambda_2 = 0.25$ for LN, and $\lambda_1 = -0.4$, $\lambda_2 = 0.7$ for QD. Here, $\gamma = 0.8$. LN and QD are measured, respectively, in ebits and bits. T/J is dimensionless,

$\{\lambda_1, \lambda_2, \gamma\}_{\mathcal{Q}}$, which results in a nonmonotonic variation of the bipartite quantum correlation measure \mathcal{Q} , with the variation of temperature. We call such a set as the “nonmonotonicity generator” (NG). Figure 6 exhibits the NGs for different values of γ , especially $\gamma = 0.2, 0.5, 0.8$, and 1.0, on the (λ_1, λ_2) plane, when LN and QD are considered to be the bipartite quantum correlation measures. We observe that in the case of LN, for low values of γ , the NGs are confined to the AFM phase and narrow regions inside the PM phase, in the vicinity of the AFM \leftrightarrow PM QPT line. At $\gamma = 0.2$, the factorization lines, denoted by the solid line on the (λ_1, λ_2) plane, almost coincide with the AFM \leftrightarrow PM QPT line, which is represented by the dashed lines. With increasing value of γ , the factorization lines get separated from the AFM \leftrightarrow PM transition lines, and the NGs span the region confined by these lines, as can be seen in the case of $\gamma = 0.5$ and 0.8. At $\gamma = 1.0$, which represents the Ising model in transverse-uniform and transverse-alternating fields, the factorization lines meet each other, and almost entire AFM phase is filled by the NGs. Remarkably, the DM phase remains completely free from NGs for all values of γ .

The behaviors of QD and LN, with respect to nonmonotonicity, are somewhat complementary to each other for low and high values of the anisotropy parameter. At $\gamma = 0.2$, NGs for QD span the PM phase, which is in contrast to the case of LN, where NGs can be found in the PM phase only in the vicinity of the AFM \leftrightarrow PM phase boundary. On the other hand, for $\gamma = 1.0$, in the case of LN, NGs fill almost the entire AFM phase while being absent in the PM and the DM phases, while in the case of QD, nonmonotonicity occurs in a very small region of the AFM and DM phases. In Fig. 7, we map, on the $(\lambda_{1(2)}, \beta J)$ plane, the regions where LN increases with decreasing the value of β which confirms the findings in Fig. 6. To generate the figures corresponding to the $(\lambda_{1(2)}, \beta J)$ plane, we have kept the value of $\lambda_{2(1)}$ fixed.

Note. In a system of finite number of spin- $\frac{1}{2}$ particles, use of the open boundary condition (OBC) instead of the PBC changes the phase boundaries only slightly, and the AFM region on the (λ_1, λ_2) plane shrinks. With an increase in the system size, the difference between the phase portraits corresponding to the PBC and the OBC reduces. Note here that each of the pairs of nearest-neighbor spins in the quantum spin model described by Eq. (1) consist of an even and an odd spin. In the case of the PBC, there is a special type of translational symmetry in the model, such that $\rho_{i,i+1} = \rho_{i+2,i+1}$, where i is,

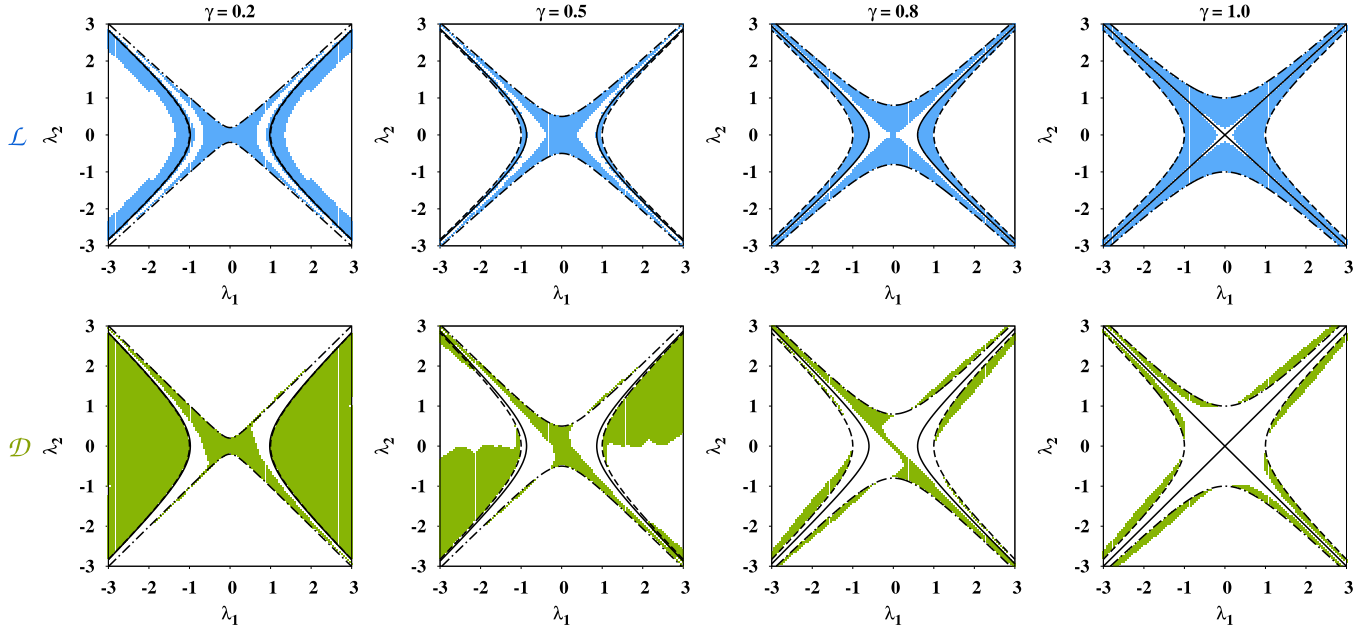


FIG. 6. Map of the regions over the (λ_1, λ_2) plane where nonmonotonic behavior of LN (figures in top horizontal panels) and QD (figures in bottom horizontal panels), with variation of temperature (marked by the shaded regions). The zero-temperature phase boundaries $\lambda_1^2 = \lambda_2^2 + 1$ (PM \leftrightarrow AFM), $\lambda_2^2 = \lambda_1^2 + \gamma^2$ (AFM \leftrightarrow DM), and the factorization line [$\lambda_1^2 = \lambda_2^2 + (1 - \gamma^2)$] are also plotted for comparison, λ_1 and λ_2 are dimensionless while LN and QD are in ebits and bits, respectively.

say, an odd site. Hence, LN is same for all the nearest-neighbor spin pairs, while due to this property, quantum discord is the same only when measurement is performed on the same type of spin (even or odd) in all nearest-neighbor spin pairs. This implies that under PBC, investigation of the bipartite quantum correlations belonging to any one of the nearest-neighbor spin pairs suffice. On the other hand, for complete characterization of the static and dynamical behavior of nearest-neighbor bipartite quantum correlations in a system of N spins under OBC, computation of bipartite quantum correlation measures corresponding to $N/2$ [$(N-1)/2$] nearest-neighbor pairs, depending on whether N is even (odd), is necessary. However, the broad qualitative features of the factorization line and the phase boundaries, as reported in this paper, remain unaltered even under OBC for finite-sized systems.

V. DYNAMICS OF QUANTUM CORRELATIONS

So far, we have considered the static characteristics of quantum correlations in different phases of the 1D anisotropic XY model in uniform and alternating transverse field. In this section, we aim to study the behavior of quantum correlations and their statistical mechanical properties under time evolution. In order to compute nearest-neighbor LN and QD of TES, the two-spin reduced density matrix has to be determined, which, in turn, requires the evaluation of single-site magnetizations and two-site spin correlation functions. This can be done by utilizing the fact that the evolutions of the subspaces in the momentum space (see Sec. II and Appendix A) are independent of each other. This leads to $\hat{\rho}^p(t) = e^{-i\hat{H}_p t} \hat{\rho}^p(0) e^{i\hat{H}_p t}$, where \hat{H}_p is the Hamiltonian in the p th momentum subspace at $t > 0$, and $\hat{\rho}^p(0) = \hat{\rho}_{eq}^p(0)$. The time-evolved single-site magnetizations and two-site spin

correlation functions are given by

$$m_{o(e)}^z(t) = \frac{2}{N} \sum_{p=1}^{N/4} \text{Tr}[\hat{m}_p^{z,o(e)} \hat{\rho}^p(t)] / \text{Tr}[\hat{\rho}^p(t)],$$

$$c^{\alpha\beta}(t) = \frac{2}{N} \sum_{p=1}^{N/4} \text{Tr}[\hat{c}_p^{\alpha\beta} \hat{\rho}^p(t)] / \text{Tr}[\hat{\rho}^p(t)]. \quad (19)$$

Note here that Eq. (19) addresses systems of finite size N . In the thermodynamic limit, the relevant quantities are obtained by replacing the sum with an proper integral, as discussed in Sec. IV. Note also that unlike the CES, $c^{xy}(t)$ and $c^{yx}(t)$ corresponding to TES do not vanish, which leads to a contribution in the c^{zz} , given by

$$c^{zz}(t) = m_o^z(t)m_e^z(t) - c^{xx}(t)c^{yy}(t) + c^{xy}(t)c^{yx}(t). \quad (20)$$

A. Ergodicity and ergodicity score

Let us now discuss the statistical mechanical properties, specifically the ergodicity of bipartite quantum correlations, in the case of the Hamiltonian given in Eq. (1). We start with a brief description and quantification of ergodicity of a generic quantum correlation measure \mathcal{Q} . A physical quantity is said to be ergodic if the time average of the quantity is the same as its ensemble average. In the present scenario, the bipartite quantum correlation \mathcal{Q} is said to be ergodic if there exists a temperature T at which the “large-time” time-averaged value of \mathcal{Q} in the TES, given by $\mathcal{Q}_\infty(T, \lambda_1, \lambda_2)$, coincides with $\mathcal{Q}_{eq}(T', \lambda_1^\infty, \lambda_2^\infty)$, the value of \mathcal{Q} in the CES at temperature T' at $t \rightarrow \infty$. Here, $\lambda_{1(2)}(t \rightarrow \infty) = \lambda_{1(2)}^\infty$. We shall shortly discuss what we mean by “large” time. Using the above definitions,

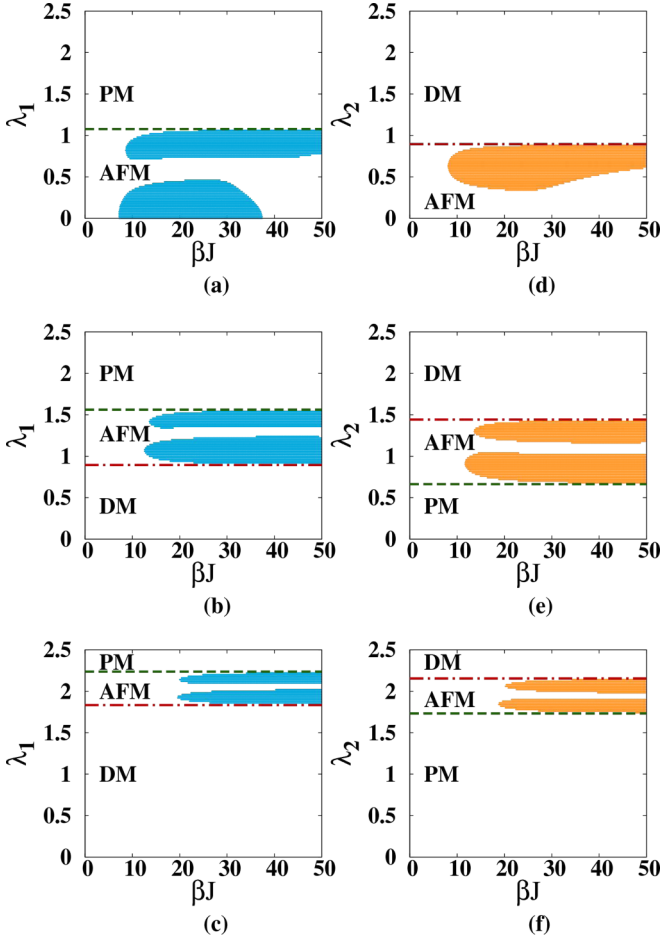


FIG. 7. Map of the regions on the $(\lambda_{1(2)}, \beta J)$ plane, where LN decreases with an increasing βJ , with the value of $\lambda_{2(1)}$ being fixed at (a), (d) $\lambda_{2(1)} = 0.4$, (b), (e) $\lambda_{2(1)} = 1.2$, and (c), (f) $\lambda_{2(1)} = 2.0$. All the other lines are same as Fig. 6. Here, λ_1 and λ_2 are dimensionless while βJ has the dimension of energy with $k_B = 1$.

one can define an “ergodicity score” as [52,53]

$$\eta_{\mathcal{S}}^{\mathcal{Q}} = \max \left[0, \mathcal{Q}_{\infty}(T, \lambda_1, \lambda_2) - \max_{T'} \mathcal{Q}_{eq}(T', \lambda_1^{\infty}, \lambda_2^{\infty}) \right], \quad (21)$$

where \mathcal{S} is the set of all system parameters $\{\lambda_1, \lambda_2, \gamma\}$, and the maximization inside the parentheses is over the physically relevant range of T' , which is up to an order of magnitude of T . Note that the value of the ergodicity score depends on all the relevant system parameters, viz., λ_1 , λ_2 , and γ , which is indicated by the subscript \mathcal{S} . As evident from the definition, a nonzero value of $\eta_{\mathcal{S}}^{\mathcal{Q}}$ implies the nonergodicity of \mathcal{Q} , while the vanishing $\eta_{\mathcal{S}}^{\mathcal{Q}}$ indicates that the quantity is ergodic.

In the case of bipartite quantum correlations, we consider the time average of the quantity at “large” time t_L . The definitions of large time may vary depending on the situation in hand. In general, we call a time instant t_L to be “large” if any one of the following scenarios occur.

(a) \mathcal{Q} saturates to \mathcal{Q}_c for $t \geq t_L$, and remains constant at $\mathcal{Q} = \mathcal{Q}_c$ for $t \geq t_L$.

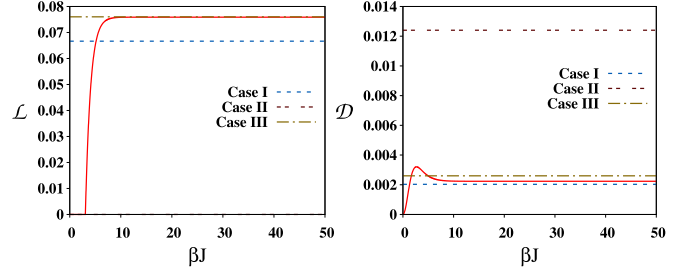


FIG. 8. Ergodicity of LN and QD for three specific cases. Case I: ($h_1 = 0.0$, $h_2 = 0.15$). Here, both LN and QD are ergodic. Case II: ($\lambda_1 = 1.0$, $\lambda_2 = 2.0$). Here, LN is ergodic, but QD is nonergodic. Case III: ($\lambda_1 = 0.15$, $\lambda_2 = 0.0$). Here, QD is clearly ergodic, while the status of LN is inconclusive, and depends on the numerical accuracy. For all the cases, initial temperature at $t = 0$ is taken to be $\beta J = 100$ at $\gamma = 0.8$. LN and QD are in ebits and bits, respectively, while βJ is dimensionless.

(b) \mathcal{Q} oscillates for $t \geq t_L$, such that $\delta_{\mathcal{Q}} \leq \delta$. Here, $\delta_{\mathcal{Q}}$ is the amplitude of fluctuation in the values of \mathcal{Q} for $t \geq t_L$, and δ is a small quantity whose value provides the required precision in determining \mathcal{Q} .

(c) For $t \geq t_L$, $\delta_{\mathcal{Q}}$ has a finite value, which remains constant in time. Evidently, the time-average is not required in the case of (a) and (b).

To determine ergodicity of the bipartite quantum correlations, as measured by LN and QD, we compute the value of $\eta_{\mathcal{S}}^{\mathcal{L}}$ and $\eta_{\mathcal{S}}^{\mathcal{D}}$, corresponding to LN and QD, respectively, for the points on the (λ_1, λ_2) plane, with different values of γ . The initial CES at $t = 0$ is chosen to be the one with $\beta J = 100$. The values of both LN and QD tend to show the behavior described in (c) for $Jt \rightarrow Jt_L$, which we found to be $\sim 100\pi$. To determine the time-averaged values of LN and QD, which depend on the choice of the values of the system parameters, we consider an interval of 20π , starting from $Jt = 100\pi$. We analyze the ergodicity properties of LN and QD via three specific cases, as follows.

In the first case (Case I), we take $\lambda_1 = 0.0$, $\lambda_2 = 0.15$, which is a point in the AFM region. In the left panel of Fig. 8, the time-averaged value of LN at large time, starting from a CES with $\beta J = 100$ at $Jt = 0$, is represented by a dashed line, which is intersected by the graph of LN varying with β (solid line). This, according to Eq. (21), implies that LN is ergodic in this case. Similar conclusion about QD can be drawn, as depicted from the right panel of Fig. 8. However, QD does not always remain ergodic, as can be seen from Case II. Here, we take a point in the DM phase, given by $\lambda_1 = 1$, $\lambda_2 = 2$, and see that the time-averaged value of LN at large time is zero (left panel, Fig. 8), leading to ergodicity of LN. In contrast, the time-averaged QD at large time, depicted by the double-dotted line in the right panel of Fig. 8, does not coincide with QD of any CES for all βJ (solid line). Hence, QD is nonergodic in this case.

The above examples naturally lead to the question as to whether bipartite entanglement in the present model is always ergodic. To verify this, we perform extensive numerical search in the parameter space of (λ_1, λ_2) . We find that that bipartite entanglement remains ergodic over the entire (λ_1, λ_2) plane,

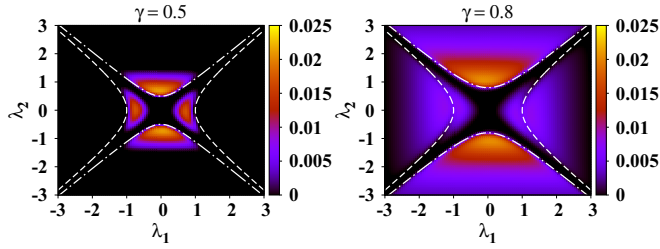


FIG. 9. Ergodicity score η_S^D , corresponding to QD, as a function of λ_1 and λ_2 for $\gamma = 0.5$ and 0.8 . The phase boundaries are the same as in Fig. 6. Here, λ_1, λ_2 are dimensionless, and η_S^D is in bits.

up to our numerical accuracy (accurate up to the third decimal place). However, there are very small sets of values of λ_1 and λ_2 for which the status of ergodicity of LN remains inconclusive. One such instance is presented by a third case, Case III. Here, $\lambda_1 = 0.15$ and $\lambda_2 = 0.0$, representing a point in the AFM phase. The corresponding time-averaged value of LN is shown by dotted-dashed line in the left panel of Fig. 8. We find that η_S^L , corresponding to LN, is zero up to the third decimal place, the point to which we claim our data to be accurate. However, there is a possibility of obtaining nonzero values of η_S^L with increased accuracy, which would imply that LN is nonergodic at $(\lambda_1 = 0.15, \lambda_2 = 0.0)$. Our numerical search suggests that the area of such regions on the (λ_1, λ_2) plane is negligibly small (cf. [52]). From exclusive numerical simulations we possibly conclude that except for $\lambda_1, \lambda_2 \approx 0$, bipartite entanglement is always ergodic irrespective of γ and low values of β of the initial state up to the numerical accuracy. In contrast, QD exhibits nonergodicity in the Case III. To investigate the ergodicity of QD over the (λ_1, λ_2) plane, we compute η_S^D , corresponding to QD, as a function of λ_1 and λ_2 . We find that the region of nonergodicity is small for small γ , and grows over the (λ_1, λ_2) plane, when the value of γ is increased. This can be understood from Fig. 9, where the plots of the values of η_S^D as function of λ_1 and λ_2 for different values of γ are depicted. We have also plotted the zero-temperature QPT lines and the separable lines for comparison. Note that even for fairly high values of γ , QD in almost the entire AFM phase remains ergodic, while the nonergodicity in QD is most prominent in the DM phase near the AFM \leftrightarrow DM QPT line.

We conclude the discussion on ergodicity with a description of the variation of time-averaged LN and QD at large time ($Jt \geq Jt_L$). Figure 10 depicts the landscape of time-averaged values of LN and QD over the (λ_1, λ_2) plane, where we have

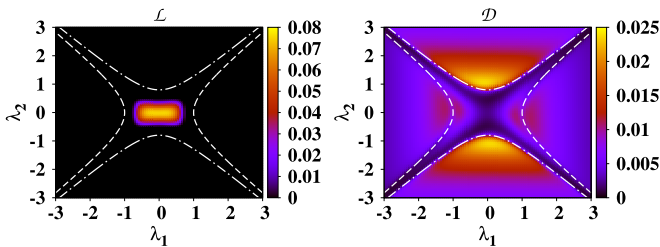


FIG. 10. Plot of the time-averaged LN (left panel) and QD (right panel) at large time as a function of λ_1 and λ_2 , which are dimensionless. The phase boundaries are same as Fig. 6. LN and QD are measured, respectively, in ebits and bits.

chosen $\gamma = 0.8$ for discussion, and the initial state of the time evolution to be the CES at $\beta J = 100$. It is clear from the figure that at $Jt \geq Jt_L$, LN persists only in the AFM region, while it vanishes completely in the entire PM and DM phases. One must note here that the definition of ergodicity score in Eq. (21) and the fact that entanglement may decrease with an increasing βJ imply that probability of finding a set of parameters, for which LN becomes nonergodic, is higher in the AFM phase where the time-averaged LN at large t has a nonzero value. This is in agreement with the Case III reported above since the parameter values $(\lambda_1 = 0.15, \lambda_2 = 0.0)$ are in the region of the (λ_1, λ_2) plane, where time-averaged value of LN at large time is high.

B. Dynamics at small time

The question of ergodicity of a physical quantity is important from the point of view of statistical mechanics. On the other hand, the information-theoretic aspects demands the study of quantum correlation in the dynamics with small time. We fix the range to $0 \leq Jt \leq 4\pi$, which is 25% of the value of Jt_L . Figures 11 and 12 depict the bird's-eye view of the landscapes of LN and QD over the (λ_1, Jt) plane, where λ_2 is constant and t is in the range of small time. For typical fixed

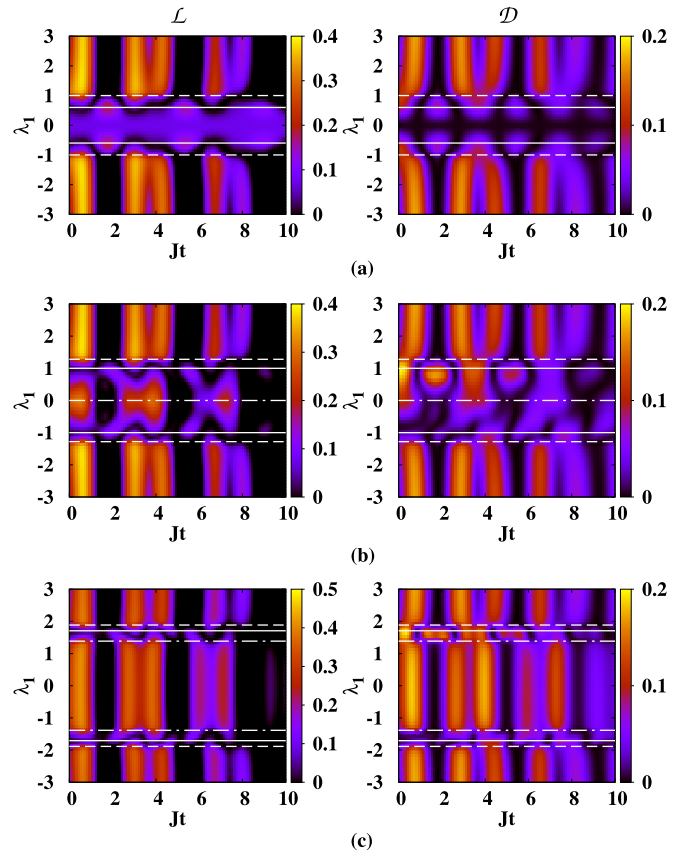


FIG. 11. Field-time landscape of LN (left panels) and QD (right panels), where λ_1 is chosen to be the varying field. Three different values of λ_2 have been chosen, viz., (a) $\lambda_2 = 0$, (b) $\lambda_2 = 0.8$, and (c) $\lambda_2 = 1.6$ with $\gamma = 0.8$. For comparison, we mark the different phases and the factorization line on the λ_1 axes (at $\beta \rightarrow \infty$), indicated by the horizontal lines, same as Fig. 6. Jt , λ_1 , and λ_2 are dimensionless. LN and QD are, respectively, in ebits and bits.

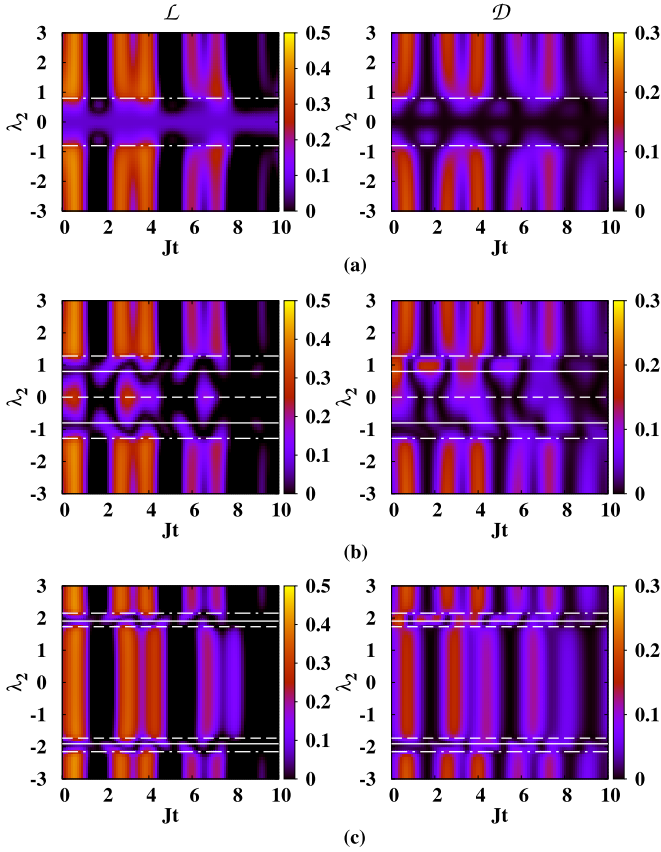


FIG. 12. Field-time landscape of LN (left panels) and QD (right panels). (a) $\lambda_1 = 0$, (b) $\lambda_1 = 0.8$, and (c) $\lambda_1 = 1.6$. All other parameters and lines are same as Fig. 11.

values of the set of system parameters given by (λ_1, λ_2) , both LN and QD are found to collapse and revive nonperiodically. It is clear from the Figs. 11 and 12 that the collapse of LN is more frequent than the collapse of QD at short time, although LN possesses much higher value.

VI. DISCUSSIONS

To summarize, we have considered a one-dimensional anisotropic XY chain of spin- $\frac{1}{2}$ spins, in the presence of a uniform and an alternating transverse field whose direction depends on whether the lattice site is even or odd. The model, via a Jordan-Wigner transformation, can be mapped onto one-dimensional two-component Fermi gas defined on an optical lattice, constituted of two sublattices consisting of the even and the odd sites. Although the analytical treatment of the model is similar to the well-known XY model, the system possesses a dimer phase apart from the paramagnetic and antiferromagnetic phases. We determine the single-site magnetizations and two-site spin correlation functions corresponding to a nearest-neighbor spin pair in canonical equilibrium state and the time-evolved state of the model, and determine the nearest-neighbor density matrix. We study the static and dynamical characteristics of nearest-neighbor entanglement quantified by LN and by investigating their variations with relevant system parameters, temperature, and time. We determine the finite-size scaling exponents

for the entanglement in the vicinity of the QPTs at zero temperature of the model. At finite temperature, we show that against increasing temperature, the bipartite entanglement is most fragile in the AFM phase, while being the most robust in the DM phase. We also demonstrate the occurrence of nonmonotonic variation of bipartite entanglement with temperature. We map the regions in different phases of the model on the plane of the chosen system parameter for which nonmonotonic variations of entanglement are found. The trend of QD which is different from entanglement in the AFM phase, the region of nonmonotonicity grows with anisotropy, and covers almost the entire AFM phase when anisotropy is high. However, the dimer phase remains completely free of such region for LN in the case of both high and low values of the anisotropy parameter has also been investigated and the measure found to be a tool for identifying phases present in this model. We find that when anisotropy in the system is low, nonmonotonicity for QD occurs mostly in the paramagnetic phase, while at high anisotropy, such regions shrink drastically.

We also consider the dynamics of the bipartite quantum correlations, as measured by LN and QD. We address the question of ergodicity of the bipartite correlations by looking into the ergodicity score corresponding to the chosen quantum correlation measure. We show that if the canonical equilibrium state at a very low temperature is chosen to be an initial state of the evolution, up to our numerical accuracy, entanglement remains ergodic over the entire phase plane of the system. On the other hand, QD can be both ergodic as well as nonergodic, suggesting an “ergodic to nonergodic” transition in the space of system parameters. Benchmarking the time at which the dynamics of the quantum correlations equilibrates, we also define a range of short time, and discuss the short-time dynamics of LN and QD for the model in focus.

ACKNOWLEDGMENTS

The Authors thank D. K. Mukherjee, S. Bhattacharyya, and S. Singha Roy for fruitful discussions, and acknowledge computations performed at the cluster computing facility of Harish-Chandra Research Institute.

APPENDIX A: DIAGONALIZATION OF THE p th SUBSPACE

The Hamiltonian \hat{H}_p that acts on the p th subspace of dimension 16 can be block-diagonalized by a choice of basis $\{|\psi_i\rangle : 1, \dots, 16\}$, given by

$$|\psi_1\rangle = a_p^\dagger b_p^\dagger |0\rangle, \quad |\psi_2\rangle = a_{-p}^\dagger b_{-p}^\dagger |0\rangle, \quad (\text{A1})$$

$$|\psi_3\rangle = a_p^\dagger |0\rangle, \quad |\psi_4\rangle = b_p^\dagger |0\rangle, \quad (\text{A2})$$

$$|\psi_5\rangle = a_p^\dagger a_{-p}^\dagger b_p^\dagger |0\rangle, \quad |\psi_6\rangle = a_p^\dagger b_p^\dagger b_{-p}^\dagger |0\rangle, \quad (\text{A3})$$

$$|\psi_7\rangle = a_{-p}^\dagger |0\rangle, \quad |\psi_8\rangle = b_{-p}^\dagger |0\rangle, \quad (\text{A3})$$

$$|\psi_9\rangle = a_p^\dagger a_{-p}^\dagger b_{-p}^\dagger |0\rangle, \quad |\psi_{10}\rangle = a_{-p}^\dagger b_p^\dagger b_{-p}^\dagger |0\rangle, \quad (\text{A3})$$

$$|\psi_{11}\rangle = a_p^\dagger b_{-p}^\dagger |0\rangle, \quad |\psi_{12}\rangle = a_{-p}^\dagger b_p^\dagger |0\rangle, \quad |\psi_{13}\rangle = a_p^\dagger a_{-p}^\dagger |0\rangle, \quad (\text{A3})$$

$$|\psi_{14}\rangle = b_p^\dagger b_{-p}^\dagger |0\rangle, \quad |\psi_{15}\rangle = a_p^\dagger a_{-p}^\dagger b_p^\dagger b_{-p}^\dagger |0\rangle, \quad |\psi_{16}\rangle = |0\rangle, \quad (\text{A4})$$

where $|0\rangle$ denotes the vacuum state. Note that the above sets of basis block-diagonalize \hat{H}_p into four blocks of dimensions 2, 4, 4, and 6, such that $\hat{H}_p = \bigoplus_{k=1}^4 \hat{H}_p^k$, which explains the above distribution of the basis vectors into four groups, given by (A1)–(A4). Using the form of \hat{H}_p [Eq. (4)] and Eqs. (A1)–(A4), \hat{H}_p^1 is found to be a null matrix of dimension 2, while $\hat{H}_p^2 = \hat{H}_p^3$, with

$$\hat{H}_p^2 = \begin{bmatrix} -h_1 - h_2 & J \cos \phi_p & -iJ\gamma \sin \phi_p & 0 \\ J \cos \phi_p & -h_1 + h_2 & 0 & -iJ\gamma \sin \phi_p \\ iJ\gamma \sin \phi_p & 0 & h_1 - h_2 & -J \cos \phi_p \\ 0 & iJ\gamma \sin \phi_p & -J \cos \phi_p & h_1 + h_2 \end{bmatrix} \quad (\text{A5})$$

and

$$\hat{H}_p^4 = \begin{bmatrix} -2h_1 & iJ\gamma \sin \phi_p & -iJ\gamma \sin \phi_p & 0 & 0 & 0 \\ -iJ\gamma \sin \phi_p & 0 & 0 & J \cos \phi_p & J \cos \phi_p & -iJ\gamma \sin \phi_p \\ iJ\gamma \sin \phi_p & 0 & 0 & -J \cos \phi_p & -J \cos \phi_p & iJ\gamma \sin \phi_p \\ 0 & J \cos \phi_p & -J \cos \phi_p & -2h_2 & 0 & 0 \\ 0 & J \cos \phi_p & -J \cos \phi_p & 0 & 2h_2 & 0 \\ 0 & iJ\gamma \sin \phi_p & -iJ\gamma \sin \phi_p & 0 & 0 & 2h_1 \end{bmatrix}. \quad (\text{A6})$$

Hence, diagonalization of the p th subspace of dimension 16 reduces to the diagonalization of the irreducible operators $\{\hat{H}_p^k, k = 1, 2, 3, 4\}$. Note that \hat{H}_p^2 and \hat{H}_p^3 provide four distinct eigenvalues in the spectrum of H_p , each of which is twofold degenerate. These four eigenvalues are given by $\pm\omega_2^\pm(p)$ where $\omega_2^\pm(p) = \sqrt{x(p) \pm 2\sqrt{y(p)}}$. Here, $x(p) = \lambda_1^2 + \lambda_2^2 + \cos^2 \phi_p + \gamma^2 \sin^2 \phi_p$ and $y(p) = \lambda_1^2(\lambda_2^2 + \cos^2 \phi_p) + \gamma^2 \lambda_2^2 \sin^2 \phi_p$, where $\lambda_{1(2)} = h_{1(2)}/J$. Two of the six eigenvalues of \hat{H}_p^4 are zero, while the other four eigenvalues are given by $\pm\omega_4^\pm(p)$, where $\omega_4^\pm(p) = 4\sqrt{x(p) \pm \sqrt{x(p)^2 - 4y(p)}}$. Clearly, $-\omega_2^+(p)$ and $-\omega_4^+(p)$ are the minimum eigenvalues of \hat{H}_p^2 and \hat{H}_p^4 , respectively. It can also be checked that $-\omega_4^+(p) \leq -\omega_2^+(p)$ irrespective of the value of p . The ground-state energy per site is obtained by $E_0 = -\frac{1}{2\pi} \int_0^{\pi/2} \omega_4^+(p) dp$.

APPENDIX B: MEASURES OF QUANTUM CORRELATIONS

We now briefly discuss two specific measures, namely, logarithmic negativity and quantum discord, belonging to entanglement-separability and quantum information-theoretic paradigms, respectively.

Negativity and logarithmic negativity. The negativity [40] $\mathcal{N}(\rho_{AB})$, for a bipartite state ρ_{AB} , is the absolute value of the sum of all the negative eigenvalues of $\rho_{AB}^{T_A}$, and is given by

$$\mathcal{N}(\rho_{AB}) = \frac{\|\rho_{AB}^{T_A}\|_1 - 1}{2}, \quad (\text{B1})$$

where $\rho_{AB}^{T_A}$ is obtained from ρ_{AB} by performing the partial transposition with respect to the subsystem A [41]. Here, $\|\rho\|_1 \equiv \text{tr} \sqrt{\rho^\dagger \rho}$ is the trace norm of the matrix ρ . The logarithmic negativity (LN) [40], $\mathcal{L}(\rho_{AB})$, defined in terms of negativity, is given by

$$\mathcal{L}(\rho_{AB}) = \log_2 [2\mathcal{N}(\rho_{AB}) + 1]. \quad (\text{B2})$$

Quantum discord. Quantum discord [43] of a bipartite quantum state ρ_{AB} is defined as the difference between the total correlation [42], quantified by the quantum mutual information, and the classical correlation present in the system.

The quantum mutual information is given by

$$\mathcal{I}(\rho_{AB}) = S(\rho_A) + S(\rho_B) - S(\rho_{AB}), \quad (\text{B3})$$

where $\rho_{A(B)}$ are the local density matrices of ρ_{AB} , obtained as $\rho_{A(B)} = \text{tr}_{B(A)}[\rho_{AB}]$, and $S(\varrho) = -\text{tr}(\varrho \log_2 \varrho)$ is the von Neumann entropy. The classical correlation of the state ρ_{AB} is defined as

$$\mathcal{J}(\rho_{AB}) = S(\rho_B) - S(\rho_{B|A}), \quad (\text{B4})$$

where $S(\rho_{B|A})$, the conditional entropy, is given by

$$S(\rho_{B|A}) = \min_{\{P_i\}} \sum_i p_i S(\rho_{B|i}). \quad (\text{B5})$$

Here, $S(\rho_{B|A})$ is conditioned over the measurements performed on A via a rank-one projective measurements $\{P_i\}$, which produces the states $\rho_{B|i} = \frac{1}{p_i} \text{tr}_A[(P_i \otimes \mathbb{I}_B)\rho_{AB}(P_i \otimes \mathbb{I}_B)]$, with probabilities $p_i = \text{tr}[(P_i \otimes \mathbb{I}_B)\rho_{AB}(P_i \otimes \mathbb{I}_B)]$, and \mathbb{I}_B is the identity operator in the Hilbert space of B . From Eqs. (B3) and (B4), quantum discord can be obtained as

$$\mathcal{D}(\rho_{AB}) = \mathcal{I}(\rho_{AB}) - \mathcal{J}(\rho_{AB}). \quad (\text{B6})$$

APPENDIX C: TWO-SITE SPIN CORRELATORS

Similar to the Hamiltonian \hat{H}_p , the two-site spin correlator operator $\hat{c}^{\alpha\alpha}$, $\alpha = x, y$, can be obtained as $\hat{c}^{\alpha\alpha} = \frac{2}{N} \sum_{p=1}^{N/4} \hat{c}_p^{\alpha\alpha}$, where in the p th subspace, $\hat{c}_p^{\alpha\alpha}$ is block-diagonalizable in the same basis as given in Appendix A. For example, one can obtain $\hat{c}^{xx} = \frac{2}{N} \sum_{i=1}^{N/2} \sigma_{2i}^x \sigma_{2i+1}^x$ corresponding to an ‘‘even-odd’’ pair of spins in the momentum space, such that

$$\begin{aligned} \hat{c}_p^{xx} = & e^{i\phi_p} (b_{-p}^\dagger a_{-p} - a_p^\dagger b_{-p}^\dagger + a_p^\dagger b_p + a_{-p} b_p) \\ & + e^{-i\phi_p} (b_p^\dagger a_p - a_{-p}^\dagger b_p^\dagger + a_{-p}^\dagger b_{-p} + a_p b_{-p}). \end{aligned} \quad (\text{C1})$$

In the basis given in Appendix A, one can write $\hat{c}_p^{\alpha\alpha} = \bigoplus_{k=1}^4 \hat{c}_p^{\alpha\alpha, k}$, where $\hat{c}_p^{\alpha\alpha, 1}$ is a null matrix of dimension 2, and

$\hat{c}_p^{xx,2}$, $\hat{c}_p^{xx,3}$, and $\hat{c}_p^{xx,4}$ are given by

$$\hat{c}_p^{xx,2} = \begin{bmatrix} 0 & e^{i\phi_p} & -e^{i\phi_p} & 0 \\ e^{-i\phi_p} & 0 & 0 & e^{-i\phi_p} \\ -e^{-i\phi_p} & 0 & 0 & -e^{-i\phi_p} \\ 0 & e^{i\phi_p} & -e^{i\phi_p} & 0 \end{bmatrix}, \quad \hat{c}_p^{xx,3} = \begin{bmatrix} 0 & e^{-i\phi_p} & e^{-i\phi_p} & 0 \\ e^{i\phi_p} & 0 & 0 & -e^{i\phi_p} \\ e^{i\phi_p} & 0 & 0 & -e^{i\phi_p} \\ 0 & -e^{-i\phi_p} & -e^{-i\phi_p} & 0 \end{bmatrix},$$

$$\hat{c}_p^{xx,4} = \begin{bmatrix} 0 & -e^{-i\phi_p} & -e^{i\phi_p} & 0 & 0 & 0 \\ -e^{i\phi_p} & 0 & 0 & e^{i\phi_p} & e^{i\phi_p} & -e^{i\phi_p} \\ -e^{-i\phi_p} & 0 & 0 & -e^{-i\phi_p} & -e^{-i\phi_p} & -e^{-i\phi_p} \\ 0 & e^{-i\phi_p} & -e^{i\phi_p} & 0 & 0 & 0 \\ 0 & e^{-i\phi_p} & -e^{i\phi_p} & 0 & 0 & 0 \\ 0 & -e^{-i\phi_p} & -e^{i\phi_p} & 0 & 0 & 0 \end{bmatrix}. \quad (C2)$$

Similar calculation for \hat{c}^{yy} leads to $\hat{c}_p^{yy,1} = c_p^{xx,1}$, and

$$\hat{c}_p^{yy,2} = \begin{bmatrix} 0 & e^{i\phi_p} & e^{i\phi_p} & 0 \\ e^{-i\phi_p} & 0 & 0 & -e^{-i\phi_p} \\ e^{-i\phi_p} & 0 & 0 & -e^{-i\phi_p} \\ 0 & -e^{i\phi_p} & -e^{i\phi_p} & 0 \end{bmatrix}, \quad \hat{c}_p^{yy,3} = \begin{bmatrix} 0 & e^{-i\phi_p} & -e^{-i\phi_p} & 0 \\ e^{i\phi_p} & 0 & 0 & e^{i\phi_p} \\ -e^{i\phi_p} & 0 & 0 & -e^{i\phi_p} \\ 0 & e^{-i\phi_p} & -e^{-i\phi_p} & 0 \end{bmatrix},$$

$$\hat{c}_p^{yy,4} = \begin{bmatrix} 0 & e^{-i\phi_p} & e^{i\phi_p} & 0 & 0 & 0 \\ e^{i\phi_p} & 0 & 0 & e^{i\phi_p} & e^{i\phi_p} & -e^{i\phi_p} \\ e^{-i\phi_p} & 0 & 0 & -e^{-i\phi_p} & -e^{-i\phi_p} & e^{-i\phi_p} \\ 0 & e^{-i\phi_p} & -e^{i\phi_p} & 0 & 0 & 0 \\ 0 & e^{-i\phi_p} & -e^{i\phi_p} & 0 & 0 & 0 \\ 0 & e^{-i\phi_p} & e^{i\phi_p} & 0 & 0 & 0 \end{bmatrix}. \quad (C3)$$

Moreover, in the case of time evolution, the operators \hat{c}^{xy} and \hat{c}^{yx} are given by

$$\hat{c}_p^{xy,2} = -i \begin{bmatrix} 0 & e^{-i\phi_p} & -e^{-i\phi_p} & 0 \\ -e^{i\phi_p} & 0 & 0 & e^{i\phi_p} \\ e^{i\phi_p} & 0 & 0 & -e^{i\phi_p} \\ 0 & -e^{-i\phi_p} & e^{-i\phi_p} & 0 \end{bmatrix}, \quad \hat{c}_p^{xy,3} = -i \begin{bmatrix} 0 & e^{-i\phi_p} & -e^{-i\phi_p} & 0 \\ e^{i\phi_p} & 0 & 0 & e^{i\phi_p} \\ -e^{i\phi_p} & 0 & 0 & -e^{i\phi_p} \\ 0 & e^{-i\phi_p} & -e^{-i\phi_p} & 0 \end{bmatrix},$$

$$\hat{c}_p^{xy,4} = -i \begin{bmatrix} 0 & e^{-i\phi_p} & e^{i\phi_p} & 0 & 0 & 0 \\ -e^{i\phi_p} & 0 & 0 & -e^{i\phi_p} & e^{i\phi_p} & e^{i\phi_p} \\ -e^{-i\phi_p} & 0 & 0 & e^{-i\phi_p} & -e^{-i\phi_p} & e^{-i\phi_p} \\ 0 & e^{-i\phi_p} & -e^{i\phi_p} & 0 & 0 & 0 \\ 0 & -e^{-i\phi_p} & e^{i\phi_p} & 0 & 0 & 0 \\ 0 & -e^{-i\phi_p} & -e^{i\phi_p} & 0 & 0 & 0 \end{bmatrix}. \quad (C4)$$

and

$$\hat{c}_p^{yx,2} = -i \begin{bmatrix} 0 & -e^{-i\phi_p} & -e^{-i\phi_p} & 0 \\ e^{i\phi_p} & 0 & 0 & e^{i\phi_p} \\ e^{i\phi_p} & 0 & 0 & e^{i\phi_p} \\ 0 & -e^{-i\phi_p} & -e^{-i\phi_p} & 0 \end{bmatrix}, \quad \hat{c}_p^{yx,3} = -i \begin{bmatrix} 0 & -e^{i\phi_p} & e^{i\phi_p} & 0 \\ e^{-i\phi_p} & 0 & 0 & -e^{-i\phi_p} \\ -e^{-i\phi_p} & 0 & 0 & e^{-i\phi_p} \\ 0 & e^{i\phi_p} & -e^{i\phi_p} & 0 \end{bmatrix},$$

$$\hat{c}_p^{yx,4} = -i \begin{bmatrix} 0 & e^{-i\phi_p} & e^{i\phi_p} & 0 & 0 & 0 \\ -e^{i\phi_p} & 0 & 0 & e^{i\phi_p} & -e^{i\phi_p} & e^{i\phi_p} \\ -e^{-i\phi_p} & 0 & 0 & -e^{-i\phi_p} & e^{-i\phi_p} & e^{-i\phi_p} \\ 0 & -e^{-i\phi_p} & e^{i\phi_p} & 0 & 0 & 0 \\ 0 & e^{-i\phi_p} & -e^{i\phi_p} & 0 & 0 & 0 \\ 0 & -e^{-i\phi_p} & -e^{i\phi_p} & 0 & 0 & 0 \end{bmatrix}, \quad (C5)$$

with $\hat{c}^{xy,1}$ and $\hat{c}^{yx,1}$ being 2×2 null matrices.

APPENDIX D: MAGNETIZATION AND CORRELATION FUNCTIONS IN CES

For the nearest-neighbor reduced density matrix at $t = 0$, one needs to determine the single-site magnetizations m_ε^z

and m_ρ^z and the diagonal elements of the correlation tensor $c^{\alpha\alpha}$ of $\rho_{eq}(t = 0)$. In order to do so, we exploit the fact that the Hilbert space of the Hamiltonian [Eq. (1)] can be decomposed into noninteracting subspaces in the momentum space. In the p th such subspace of the momentum space, the

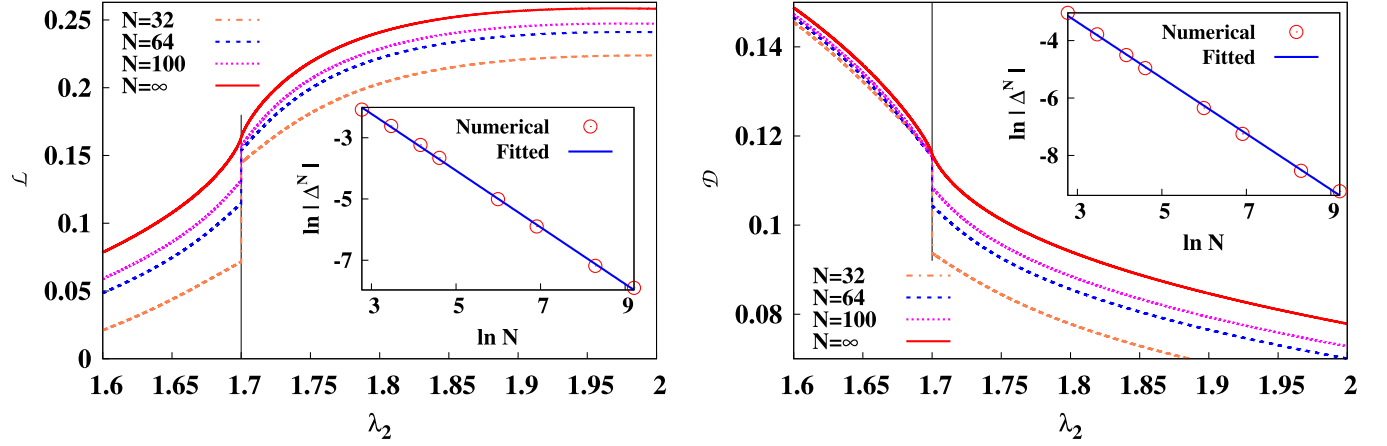


FIG. 13. The figure in the left (right) panel depicts the variation of \mathcal{L} (\mathcal{D}) with λ_2 across the AFM \leftrightarrow DM QPT for different values of N , with $\lambda_1 = 1.5$. At the QPT point, the quantum correlations exhibit a finite jump in magnitude, given by Δ^N . (Insets) Corresponding variations of $\ln |\Delta^N|$ (both numerical data and fitted line) as a function of $\ln N$. All the quantities plotted are dimensionless, except LN which is in ebits and QD which is in bits.

CES can be written as $\rho_{eq}^p = \exp[-\beta \hat{H}_p(t=0)]/Z_p$, where $Z_p = \text{Tr}\{\exp[-\beta \hat{H}_p(t=0)]\}$ is the partition function in that momentum subspace. Using the form of ρ_{eq}^p , equilibrium expectation value of an operator \hat{O}_p can be obtained as

$$\langle \hat{O} \rangle = \frac{2}{N} \sum_{p=1}^{N/4} \text{Tr}[\hat{O}_p \rho_{eq}^p] / \text{Tr}[\rho_{eq}^p]. \quad (\text{D1})$$

From the transformation scheme described in Sec. II, the transverse magnetization operator in momentum space for an odd (even) site can be calculated as $\hat{m}_p^z = 2(c_p^\dagger c_p + c_{-p}^\dagger c_{-p} - 1)$, where $c \equiv a$ (odd site) or $c \equiv b$ (even site). We find that, similar to \hat{H}_p , the two-site correlator operators $\hat{c}^{\alpha\alpha}$, $\alpha = x, y$, can be written as $\hat{c}^{\alpha\alpha} = \frac{2}{N} \sum_{p=1}^{N/4} \hat{c}_p^{\alpha\alpha}$, where $\hat{c}_p^{\alpha\alpha}$ can be expanded in the same basis as described in Appendix A. The forms of the operators $\hat{c}_p^{\alpha\alpha}$, in the momentum space, are given in Appendix C. Unlike \hat{c}^{xx} and \hat{c}^{yy} , \hat{c}^{zz} can not be obtained directly due to the presence of the four-fermionic terms in its expansion, but its expectation value c^{zz} can be obtained from the relation

$$c^{zz} = m_o^z m_e^z - c^{xx} c^{yy} \quad (\text{D2})$$

for the thermal state including the zero-temperature state. Here, we denote the expectation values of the respective operators by the same symbol without the hat. Note that in the thermodynamic limit $N \rightarrow \infty$, the sum in Eq. (D1) is replaced by an integral with proper limit in the reduced Brillouin zone, such that Eq. (D1) reads as

$$\langle \hat{O} \rangle = \frac{1}{\pi} \int_0^{\frac{\pi}{2}} \text{Tr}[\hat{O}_p \rho_{eq}^p] / \text{Tr}[\rho_{eq}^p] d\phi_p. \quad (\text{D3})$$

APPENDIX E: AFM TO DM TRANSITION

While investigating the AFM \leftrightarrow DM QPT, one may try to determine the zero-temperature canonical equilibrium state ρ_{eo} corresponding to a nearest-neighbor even-odd spin pair, by using the methodology discussed in Sec. II B. However, due to the approximations in the calculation, the variations of LN and

QD exhibit finite jumps at the QPT point for fixed finite values of the system size N . This imposes a restriction in analyzing the finite-size scaling behavior using the usual procedure as discussed in the case of the AFM \leftrightarrow DM. To understand this feature of the approximations properly, let us denote the value of the quantum correlation measure (which, in the present case, is either LN or QD) by $Q_{-\delta}$, when $\lambda_{1(2)} = \lambda_{1(2)}^c - \delta$ with arbitrarily small $\delta (\rightarrow 0)$, while the same for $\lambda_{1(2)} = \lambda_{1(2)}^c + \delta$ is given by $Q_{+\delta}$. We find the trends of absolute value of the difference between $Q_{\pm\delta}$ for a fixed value of N , denoted by Δ^N and it approaches zero with increasing N as

$$|\Delta^N| = \tilde{\alpha}_{1(2)} N^{-\tilde{\nu}_{1(2)}}, \quad (\text{E1})$$

where $\tilde{\alpha}_{1(2)}$ is a dimensionless constant. Note that the subscript “1(2)” indicates the choice of $\lambda_1(\lambda_2)$ as the tuning parameter. Insets of Fig. 13 depict the variations of $\ln |\Delta^N|$ as a function of $\ln N$. Values of $\tilde{\alpha}_{1(2)}$ and $\tilde{\nu}_{1(2)}$ can be estimated by fitting the numerical data with Eq. (E1). The values of $\tilde{\alpha}$ and $\tilde{\nu}$ for LN and

TABLE II. The fitting parameters corresponding to the finite jumps of LN and QD at the AFM \leftrightarrow DM transition point, arising out of the approximations used in the analysis. For all the computations, $\gamma = 0.8$.

Tuning parameter: λ_2		
λ_1	LN	QD
0.0	$\tilde{\nu}_2 = 0.992 \pm 0.010$	$\tilde{\nu}_2 = 0.893 \pm 0.018$
	$\ln \tilde{\alpha}_2 = 1.357 \pm 0.065$	$\ln \tilde{\alpha}_2 = -1.453 \pm 0.132$
1.5	$\tilde{\nu}_2 = 0.926 \pm 0.010$	$\tilde{\nu}_2 = 0.972 \pm 0.015$
	$\ln \tilde{\alpha}_2 = 0.559 \pm 0.063$	$\ln \tilde{\alpha}_2 = -0.443 \pm 0.092$
Tuning parameter: λ_1		
λ_2	LN	QD
1.5	$\tilde{\nu}_1 = 0.942 \pm 0.009$	$\tilde{\nu}_1 = 0.988 \pm 0.013$
	$\ln \tilde{\alpha}_1 = 0.721 \pm 0.054$	$\ln \tilde{\alpha}_1 = -0.286 \pm 0.082$

QD are given in Table II, where the values of λ_2 (λ_1) are kept fixed at $\lambda_1 = 0$ and 1.5 ($\lambda_2 = 1.5$). This analysis indicates that the approximations are too drastic to investigate the intricacies

of the AFM \leftrightarrow DM transitions in the model. However, as expected, the effect of the approximations tends to disappear with increasing N .

-
- [1] L. Amico, R. Fazio, A. Osterloh, and V. Vedral, *Rev. Mod. Phys.* **80**, 517 (2008).
- [2] M. Lewenstein, A. Sanpera, V. Ahufinger, B. Damski, A. Sen (De), and U. Sen, *Adv. Phys.* **56**, 243 (2006).
- [3] H. J. Briegel, D. E. Browne, W. Dür, R. Raussendorf, and M. V. den Nest, *Nat. Phys.* **5**, 19 (2009).
- [4] S. Bose, *Phys. Rev. Lett.* **91**, 207901 (2003); V. Subrahmanyam, *Phys. Rev. A* **69**, 034304 (2004); D. Burgarth, S. Bose, and V. Giovannetti, *Int. J. Quantum Inf.* **04**, 405 (2006); Z.-M. Wang, M. S. Byrd, B. Shao, and J. Zou, *Phys. Lett. A* **373**, 636 (2009); P. J. Pemberton-Ross and A. Kay, *Phys. Rev. Lett.* **106**, 020503 (2011); N. Y. Yao, L. Jiang, A. V. Gorshkov, Z.-X. Gong, A. Zhai, L.-M. Duan, and M. D. Lukin, *ibid.* **106**, 040505 (2011); H. Yadsan-Appléby and T. J. Osborne, *Phys. Rev. A* **85**, 012310 (2012); T. J. G. Apollaro, S. Lorenzo, and F. Plastina, *Int. J. Mod. Phys. B* **27**, 1345035 (2013).
- [5] O. Mandel, M. Greiner, A. Widera, T. Rom, T. W. Hänsch, and I. Bloch, *Nature (London)* **425**, 937 (2003); I. Bloch, *J. Phys. B: At., Mol. Opt. Phys.* **38**, S629 (2005); P. Treutlein, T. Steinmetz, Y. Colombe, B. Lev, P. Hommelhoff, J. Reichel, M. Greiner, O. Mandel, A. Widera, T. Rom, I. Bloch, and T. W. Hänsch, *Fortschr. Phys.* **54**, 702 (2006); M. Cramer, A. Bernard, N. Fabbri, L. Fallani, C. Fort, S. Rosi, F. Caruso, M. Inguscio, and M. B. Plenio, *Nat. Commun.* **4**, 2161 (2013), and references therein.
- [6] J. Struck, C. Ölschläger, R. Le Targat, P. Soltan-Panahi, A. Eckardt, M. Lewenstein, P. Windpassinger, and K. Sengstock, *Science* **333**, 996 (2011); J. Simon, W. S. Bakr, R. Ma, M. E. Tai, P. M. Preiss, and M. Greiner, *Nature (London)* **472**, 307 (2011), and references therein.
- [7] J.-J. García-Ripoll and J. I. Cirac, *New J. Phys.* **5**, 76 (2003); L.-M. Duan, E. Demler, and M. D. Lukin, *Phys. Rev. Lett.* **91**, 090402 (2003), and references therein.
- [8] D. Leibfried, R. Blatt, C. Monroe, and D. Wineland, *Rev. Mod. Phys.* **75**, 281 (2003); X.-L. Deng, D. Porras, and J. I. Cirac, *Phys. Rev. A* **72**, 063407 (2005); H. Häffner, C. Roos, and R. Blatt, *Phys. Rep.* **469**, 155 (2008); K. Kim, M.-S. Chang, S. Korenblit, R. Islam, E. E. Edwards, J. K. Freericks, G.-D. Lin, L.-M. Duan, and C. Monroe, *Nature (London)* **465**, 590 (2010); R. Islam, E. E. Edwards, K. Kim, S. Korenblit, C. Noh, H. Carmichael, G.-D. Lin, L.-M. Duan, C.-C. Joseph Wang, J. K. Freericks, and C. Monroe, *Nat. Commun.* **2**, 377 (2011); J. Struck, M. Weinberg, C. Ölschläger, P. Windpassinger, J. Simonet, K. Sengstock, R. Höppner, P. Hauke, A. Eckardt, M. Lewenstein, and L. Mathey, *Nat. Phys.* **9**, 738 (2013), and references therein.
- [9] M. Schechter and P. C. E. Stamp, *Phys. Rev. B* **78**, 054438 (2008), and references therein.
- [10] L. M. K. Vandersypen and I. L. Chuang, *Rev. Mod. Phys.* **76**, 1037 (2005); J. Zhang, M.-H. Yung, R. Laflamme, A. Aspuru-Guzik, and J. Baugh, *Nat. Commun.* **3**, 880 (2012); K. R. K. Rao, H. Katiyar, T. S. Mahesh, A. Sen De, U. Sen, and A. Kumar, *Phys. Rev. A* **88**, 022312 (2013), and references therein.
- [11] R. Horodecki, P. Horodecki, M. Horodecki, and K. Horodecki, *Rev. Mod. Phys.* **81**, 865 (2009).
- [12] K. Modi, A. Brodutch, H. Cable, T. Patrek, and V. Vedral, *Rev. Mod. Phys.* **84**, 1655 (2012).
- [13] G. Vidal, *Phys. Rev. Lett.* **91**, 147902 (2003); **93**, 040502 (2004).
- [14] S. R. White, *Phys. Rev. Lett.* **69**, 2863 (1992); *Phys. Rev. B* **48**, 10345 (1993); U. Schollwöck, *Rev. Mod. Phys.* **77**, 259 (2005).
- [15] F. Verstraete, D. Porras, and J. I. Cirac, *Phys. Rev. Lett.* **93**, 227205 (2004).
- [16] W. Ogburn and J. Preskill, *Lect. Notes Comput. Sci.* **1509**, 341 (1999); A. Kitaev, *Ann. Phys. (NY)* **303**, 2 (2003); M. H. Freedman, A. Kitaev, M. J. Larsen, and Z. Wang, *Bull. Am. Math. Soc.* **40**, 31 (2003); S. Das Sarma, M. Freedman, and C. Nayak, *Phys. Today* **59**(7), 32 (2006); R. Raussendorf and J. Harrington, *Phys. Rev. Lett.* **98**, 190504 (2007); R. Raussendorf, J. Harrington, and K. Goyal, *New J. Phys.* **9**, 199 (2007); C. Nayak, S. H. Simon, A. Stern, M. Freedman, and S. Das Sarma, *Rev. Mod. Phys.* **80**, 1083 (2008); X.-C. Yao, T.-X. Wang, H.-Z. Chen, W.-B. Gao, A. G. Fowler, R. Raussendorf, Z.-B. Chen, N.-L. Liu, C.-Y. Lu, Y.-J. Deng, Y.-A. Chen, and J.-W. Pan, *Nature (London)* **482**, 489 (2012).
- [17] B. K. Chakrabarti, A. Dutta, and P. Sen, *Quantum Ising Phases and Transitions in Transverse Ising Models* (Springer, Heidelberg, 1996); S. Sachdev, *Quantum Phase Transitions* (Cambridge University Press, Cambridge, 2011); S. Suzuki, J.-I. Inou, and B. K. Chakrabarti, *Quantum Ising Phases and Transitions in Transverse Ising Models* (Springer, Heidelberg, 2013).
- [18] A. Dutta, G. Aeppli, B. K. Chakrabarti, U. Divakaran, T. F. Rosenbaum, and D. Sen, *Quantum Phase Transitions in Transverse Field Spin Models: From Statistical Physics to Quantum Information* (Cambridge University Press, Cambridge, 2015).
- [19] J. I. Latorre and A. Riera, *J. Phys. A: Math. Theor.* **42**, 504002 (2009).
- [20] J. Eisert, M. Cramer, and M. B. Plenio, *Rev. Mod. Phys.* **82**, 277 (2010).
- [21] D. Gunlycke, V. M. Kendon, V. Vedral, and S. Bose, *Phys. Rev. A* **64**, 042302 (2001); T. J. Osborne and M. A. Nielsen, *ibid.* **66**, 032110 (2002); G. Vidal, J. I. Latorre, E. Rico, and A. Kitaev, *Phys. Rev. Lett.* **90**, 227902 (2003); T.-C. Wei, D. Das, S. Mukhopadhyay, S. Vishveshwara, and P. M. Goldbart, *Phys. Rev. A* **71**, 060305(R) (2005); L. Zhang and P. Tong, *J. Phys. A: Math. Gen.* **38**, 7377 (2005); T. R. de Oliveira, G. Rigolin, M. C. de Oliveira, and E. Miranda, *Phys. Rev. Lett.* **97**, 170401 (2006); T. R. de Oliveira, G. Rigolin, and M. C. de Oliveira, *Phys. Rev. A* **73**, 010305(R) (2006); **74**, 039902(E) (2006); **75**, 039901(E) (2007); S. M. Giampaolo and B. C. Hiesmayr, *ibid.* **88**, 052305 (2013); Z.-Y. Sun, Y.-Y. Wu, J. Xu, H.-L. Huang, B.-F. Zhan, B. Wang, and C.-B. Duan, *ibid.* **89**, 022101 (2014).
- [22] O. F. Syljuasen, *Phys. Rev. A* **68**, 060301 (2003).
- [23] R. Dillenschneider, *Phys. Rev. B* **78**, 224413 (2008); M. S. Sarandy, *Phys. Rev. A* **80**, 022108 (2009); T. Nag, A. Patra, and

- A. Dutta, *J. Stat. Mech.* (2011) P08026; J. Maziero, L. C. Céleri, R. M. Serra, and M. S. Sarandy, *Phys. Lett. A* **376**, 1540 (2012); B. Tomasello, D. Rossini, A. Hamma, and L. Amico, *Int. J. Mod. Phys. B* **26**, 1243002 (2012); H. S. Dhar, R. Ghosh, A. Sen (De), and U. Sen, *Europhys. Lett.* **98**, 30013 (2012); S. Campbell, L. Mazzola, G. D. Chiara, T. J. G. Apollaro, F. Plastina, T. Bush, and M. Paternostro, *New J. Phys.* **15**, 043033 (2013); T. Nag, A. Dutta, and A. Patra, *Int. J. Mod. Phys. B* **27**, 1345036 (2013).
- [24] H. A. Bethe, *Z. Phys.* **71**, 205 (1931); C. N. Yang and C. P. Yang, *Phys. Rev.* **150**, 321 (1966); **150**, 327 (1966); A. Langari, *Phys. Rev. B* **58**, 14467 (1998); M. Takahashi, *Thermodynamics of One-Dimensional Solvable Models* (Cambridge University Press, Cambridge, 1999); D. V. Dmitriev, V. Y. Krivnov, A. A. Ovchinnikov, and A. Langari, *J. Exp. Theor. Phys.* **95**, 538 (2002); H.-J. Mikeska and A. K. Kolezhuk, *Lect. Notes Phys.* **645**, 1 (2004); S. Mahdaviifar, *J. Phys.: Condens. Matter* **19**, 406222 (2007).
- [25] M. C. Arnesen, S. Bose, and V. Vedral, *Phys. Rev. Lett.* **87**, 017901 (2001).
- [26] X. Wang, *Phys. Rev. A* **66**, 034302 (2002); G. L. Kamta and A. F. Starace, *Phys. Rev. Lett.* **88**, 107901 (2002); S. Scheel, J. Eisert, P. L. Knight, and M. B. Plenio, *J. Mod. Opt.* **50**, 881 (2003); F. K. Fumania, S. Nematib, S. Mahdaviifar, and A. H. Daroonehb, *Phys. A (Amsterdam)* **445**, 256 (2016).
- [27] X. Wang, H. Fu, and A. I. Solomon, *J. Phys. A: Math. Gen.* **34**, 11307 (2001); X. Wang, *Phys. Rev. A* **66**, 044305 (2002); S.-J. Gu, H.-Q. Lin, and Y.-Q. Li, *ibid.* **68**, 042330 (2003); J. Vidal, R. Mosseri, and J. Dukelsky, *ibid.* **69**, 054101 (2004); L. A. Wu, M. S. Sarandy, and D. A. Lidar, *Phys. Rev. Lett.* **93**, 250404 (2004).
- [28] T. Werlang and G. Rigolin, *Phys. Rev. A* **81**, 044101 (2010); T. Werlang, C. Trippé, G. A. P. Ribeiro, and G. Rigolin, *Phys. Rev. Lett.* **105**, 095702 (2010); T. Werlang, G. A. P. Ribeiro, and G. Rigolin, *Phys. Rev. A* **83**, 062334 (2011); *Int. J. Mod. Phys. B* **27**, 1345032 (2013).
- [29] M. Lewenstein, L. Santos, M. A. Baranov, and H. Fehrmann, *Phys. Rev. Lett.* **92**, 050401 (2004).
- [30] E. Lieb, T. Schultz, and D. Mattis, *Ann. Phys. (NY)* **16**, 407 (1961).
- [31] E. Barouch, B. McCoy, and M. Dresden, *Phys. Rev. A* **2**, 1075 (1970); E. Barouch and B. McCoy, *ibid.* **3**, 786 (1971).
- [32] E. A. Cornell and C. E. Wieman, *Rev. Mod. Phys.* **74**, 875 (2002); N. Ketterle, *ibid.* **74**, 1131 (2002).
- [33] T. Jelts, J. M. McNamara, W. Hogervorst, W. Vassen, V. Krachmalnicoff, M. Schellekens, A. Perrin, H. Chang, D. Boiron, A. Aspect, and C. I. Westbrook, *Nature (London)* **445**, 402 (2007); I. Bloch, J. Dalibard, and W. Zwerger, *Rev. Mod. Phys.* **80**, 885 (2008); A. Polkovnikov, K. Sengupta, A. Silva, and M. Vengalattore, *ibid.* **83**, 863 (2011).
- [34] G. Modugno, M. Modugno, F. Riboli, G. Roati, and M. Inguscio, *Phys. Rev. Lett.* **89**, 190404 (2002); G. Modugno, F. Ferlaino, R. Heidemann, G. Roati, and M. Inguscio, *Phys. Rev. A* **68**, 011601(R) (2003); M. Köhl, H. Moritz, T. Stöferle, K. Günter, and T. Esslinger, *Phys. Rev. Lett.* **94**, 080403 (2005); T. Stöferle, H. Moritz, K. Günter, M. Köhl, and T. Esslinger, *ibid.* **96**, 030401 (2006); S. Ospelkaus, C. Ospelkaus, L. Humbert, K. Sengstock, and K. Bongs, *ibid.* **97**, 120403 (2006).
- [35] J. K. Chin, D. E. Miller, Y. Liu, C. Stan, W. Setiawan, C. Sanner, K. Xu, and W. Ketterle, *Nature (London)* **443**, 961 (2006); U. Schneider, L. Hackermüller, S. Will, Th. Best, I. Bloch, T. A. Costi, R. W. Helmes, D. Rasch, and A. Rosch, *Science* **322**, 1520 (2008); R. Jördens, N. Strohmaier, K. Günter, H. Moritz, and T. Esslinger, *Nature (London)* **455**, 204 (2008).
- [36] J. B. Kogut, *Rev. Mod. Phys.* **51**, 659 (1979).
- [37] J. H. H. Perk, H. W. Capel, and M. J. Zuilhof, *Phys. A (Amsterdam)* **81**, 319 (1975); K. Okamoto and K. Yasumura, *J. Phys. Soc. Jpn.* **59**, 993 (1990).
- [38] U. Divakaran, A. Dutta, and D. Sen, *Phys. Rev. B* **78**, 144301 (2008); S. Deng, G. Ortiz, and L. Viola, [arXiv:0802.3941](https://arxiv.org/abs/0802.3941).
- [39] H. T. Diep, *Frustrated Spin Systems* (University of Cergy-Pontoise, France, 2005).
- [40] K. Życzkowski, P. Horodecki, A. Sanpera, and M. Lewenstein, *Phys. Rev. A* **58**, 883 (1998); J. Lee, M. S. Kim, Y. J. Park, and S. Lee, *J. Mod. Opt.* **47**, 2151 (2000); G. Vidal and R. F. Werner, *Phys. Rev. A* **65**, 032314 (2002); M. B. Plenio, *Phys. Rev. Lett.* **95**, 090503 (2005).
- [41] A. Peres, *Phys. Rev. Lett.* **77**, 1413 (1996); M. Horodecki, P. Horodecki, and R. Horodecki, *Phys. Lett. A* **223**, 1 (1996).
- [42] W. H. Zurek, in *Quantum Optics, Experimental Gravitation and Measurement Theory*, edited by P. Meystre and M. O. Scully (Plenum, New York, 1983); S. M. Barnett and S. J. D. Phoenix, *Phys. Rev. A* **40**, 2404 (1989); B. Schumacher and M. A. Nielsen, *ibid.* **54**, 2629 (1996); N. J. Cerf and C. Adami, *Phys. Rev. Lett.* **79**, 5194 (1997); B. Groomsman, S. Popescu, and A. Winter, *Phys. Rev. A* **72**, 032317 (2005).
- [43] L. Henderson and V. Vedral, *J. Phys. A: Math. Gen.* **34**, 6899 (2001); H. Ollivier and W. H. Zurek, *Phys. Rev. Lett.* **88**, 017901 (2001).
- [44] J. Kurmann, H. Thomas, G. Müller, M. W. Puga, and H. Bech, *J. Appl. Phys.* **52**, 1968 (1981); J. Kurmann, H. Thomas, and G. Müller, *Phys. A (Amsterdam)* **112**, 235 (1982); J. E. Bunder and R. H. McKenzie, *Phys. Rev. B* **60**, 344 (1999); *Phys. Rev. Lett.* **77**, 4804 (1996).
- [45] M. R. Dowling, A. C. Doherty, and S. D. Bartlett, *Phys. Rev. A* **70**, 062113 (2004); T. Roscilde, P. Verrucchi, A. Fubini, S. Haas, and V. Tognetti, *Phys. Rev. Lett.* **93**, 167203 (2004); **94**, 147208 (2005); L. Amico, F. Baroni, A. Fubini, D. Patane, V. Tognetti, and P. Verrucchi, *Phys. Rev. A* **74**, 022322 (2006); F. Baroni, A. Fubini, V. Tognetti, and P. Verrucchi, *J. Phys. A: Math. Theor.* **40**, 9845 (2007); S. M. Giampaolo, G. Adesso, and F. Illuminati, *Phys. Rev. Lett.* **100**, 197201 (2008); R. Rossignoli, N. Canosa, and J. M. Matera, *Phys. Rev. A* **77**, 052322 (2008); S. M. Giampaolo, G. Adesso, and F. Illuminati, *Phys. Rev. B* **79**, 224434 (2009); G. L. Giorgi, *ibid.* **79**, 060405(R) (2009); R. Rossignoli, N. Canosa, and J. M. Matera, *Phys. Rev. A* **80**, 062325 (2009); S. M. Giampaolo, G. Adesso, and F. Illuminati, *Phys. Rev. Lett.* **104**, 207202 (2010); B. Cakmak, G. Karpat, and F. F. Fanchini, *Entropy* **17**, 790 (2015).
- [46] The usual statistical mechanical description of a physical quantity is applicable when the quantity is *ergodic*, i.e., the time average of the quantity matches with its ensemble average.
- [47] P. Mazur, *Physica (Amsterdam)* **43**, 533 (1969).
- [48] J. H. H. Perk, H. W. Capel, and Th. J. Sisken, *Physica (Amsterdam)* **89**, 304 (1977); J. H. H. Perk and H. Au-Yang, *J. Stat. Phys.* **135**, 599 (2009).
- [49] T. Prosen, *Phys. Rev. E* **60**, 3949 (1999); E. Plekhanov, A. Avella, and F. Mancini, *Phys. Rev. B* **74**, 115120 (2006); S. Deng, G. Ortiz, and L. Viola, *Europhys. Lett.* **84**, 67008 (2008);

- [Phys. Rev. B **80**, 241109\(R\) \(2009\)](#); M. Znidaric, T. Prosen, G. Benenti, G. Casati, and D. Rossini, [Phys. Rev. E **81**, 051135 \(2010\)](#); G. Sadiq, Q. Xu, and S. Kais, [Phys. Rev. A **85**, 042313 \(2012\)](#); A. D. Luca and A. Scardicchio, [Europhys. Lett. **101**, 37003 \(2013\)](#).
- [50] L. Amico, A. Osterloh, F. Plastina, R. Fazio, and G. M. Palma, [Phys. Rev. A **69**, 022304 \(2004\)](#).
- [51] A. Sen(De), U. Sen, and M. Lewenstein, [Phys. Rev. A **72**, 052319 \(2005\)](#).
- [52] R. Prabhu, A. Sen (De), and U. Sen, [Phys. Rev. A **86**, 012336 \(2012\)](#).
- [53] R. Prabhu, A. Sen (De), and U. Sen, [Europhys. Lett. **102**, 30001 \(2013\)](#).
- [54] U. Mishra, R. Prabhu, A. Sen (De), and U. Sen, [Phys. Rev. A **87**, 052318 \(2013\)](#).
- [55] M.-F. Yang, [Phys. Rev. A. **71**, 030302 \(2005\)](#); X.-F. Qian, T. Shi, Y. Li, Z. Song, and C.-P. Sun, [ibid. **72**, 012333 \(2005\)](#).
- [56] R. W. Chhajlany, P. Tomczak, A. Wójcik, and J. Richter, [Phys. Rev. A **75**, 032340 \(2007\)](#); A. Biswas, R. Prabhu, A. Sen (De), and U. Sen, [ibid. **90**, 032301 \(2014\)](#).
- [57] C. Lanczos, [J. Res. Natl. Bur. Stand. **45**, 255 \(1950\)](#).